THESIS

IMPROVING A SNOW ENERGY AND MASS BALANCE MODEL WITH OBSERVATIONS OF ALBEDO DECAY AND RECOVERY FOLLOWING COLORADO'S 2020 CAMERON PEAK WILDFIRE

Submitted by

Noah G. Caldwell

Department of Geosciences

In partial fulfillment of requirements

For the Degree of Master of Science

Colorado State University

Fort Collins, Colorado

Summer 2026

Master's Committee:

Advisor: Daniel McGrath

Steven Fassnacht
Michael Ronayne

ABSTRACT

IMPROVING A SNOW ENERGY AND MASS BALANCE MODEL WITH OBSERVATIONS OF ALBEDO DECAY AND RECOVERY FOLLOWING COLORADO'S 2020 CAMERON PEAK WILDFIRE

Wildfires have grown in both intensity and extent, with recent events increasingly affecting seasonal snow zones that accumulate deep, persistent snowpacks. Post-fire impacts—such as forest canopy loss and deposition of light-absorbing impurities (e.g., charred debris and soot)—increase net shortwave radiation to the snowpack by diminishing canopy shading and reducing snow albedo, resulting in accelerated snowmelt and earlier snow disappearance. While previous work has shown that snow albedo can gradually recover, the rate and magnitude of recovery remain poorly constrained in physically based snow models. This study analyzes observations of albedo decay and recovery following Colorado's 2020 Cameron Peak Fire, the largest wildfire in state history. Station-measured albedo indicated that median ablation-season albedo increased by ~40% during the study period (0.38 in WY 2022 to 0.53 in WY 2025). Event-scale analysis showed faster and more variable albedo decay following snowfall at burned sites, with median decay rates up to ~2–3 times more negative than unburned sites. These observations inform updates to post-fire albedo decay parameterization in iSnobal, a snow energy and mass balance model. Compared to the base configuration, implementing a new exponential albedo decay method improved agreement with observed albedo distributions by 50–63% during water years 2021–2023 and shifted modeled snow disappearance 8–14 days closer to observations. iSnobal simulations demonstrated that canopy loss exerted a stronger and more persistent control on net

shortwave energy absorption than post-fire albedo changes. Accounting for post-wildfire canopy loss and albedo changes in snow models is critical for predicting snowmelt timing and water yield in fire-affected regions.

ACKNOWLEDGEMENTS

The work presented here for my master's thesis would not have been possible without the generous support and contributions of many individuals. First, I thank my advisor Dr. Daniel McGrath for taking me on as a new research student at Colorado State University, and for continuous guidance and support throughout this project. His mentorship challenged me to produce rigorous science. Thank you to Dr. Joachim Meyer at Boise State University for his assistance with implementing and running the iSnobal model, and for thoughtful feedback throughout the writing process and interpretation of puzzling modeling behavior. I would also like to acknowledge the broader iSnobal community for supporting advancement of the model and for providing thoughtful feedback during community meetings and in person at the 2026 AGU conference meeting in New Orleans.

Field data collection for this project would not have been possible without the dedication of many individuals who endured long and often harsh winter conditions at Cameron Pass. I thank Will Selvidge, Haley Boron, Ashlesha Khatiwada, Sushma Tiwari Chhetri, Mia Morones, Nate Sievers, Taylor Stoudnour, Wyatt Reis, Ally Detre, Helen Flynn, and Arielle Koshkin for their assistance.

I am deeply grateful to my friends and family that have supported me through my graduate school journey at CSU. I especially thank my fellow CSU Cryosphere Sciences Research Group members, Helen, Ash, Ally, and Haley for their friendship, encouragement, and creating a supportive and collaborative environment.

This research was funded by the U.S. Bureau of Reclamation Snow Water Supply Forecasting Program (Grant No. R24AC00027).

TABLE OF CONTENTS

LIST OF TABLES

LIST OF FIGURES

LIST OF EQUATIONS

1. INTRODUCTION

1.1. Snowpack Response to Warming and Implications for Water Resources

Seasonal snow cover is a fundamental component of the Earth system, influencing both surface energy balance and hydrologic processes. Snow-covered surfaces have a high albedo, which reflects a large fraction of incoming solar radiation back into the atmosphere, reducing absorbed shortwave radiation at the surface and acting as a key control on land-atmosphere energy interactions (Skiles et al., 2018). In snow-dominated regions, seasonal snow serves a critical hydrologic role by storing winter precipitation and regulating the timing and magnitude of runoff, linking atmospheric processes to downstream water availability (Barnett et al., 2005; Li et al., 2017). Because of this role in both climate and hydrologic systems, changes in snow accumulation and melt processes have important implications for climate feedback and water resources (Barnett et al., 2005; Li et al., 2017).

Warming winter temperatures are significantly altering snowpack dynamics, including reduced magnitude and earlier timing of peak snow water equivalent (SWE) and earlier snow-disappearance dates (SDD) in seasonal snow-covered landscapes (Clow, 2010; Hale et al., 2023; Mote et al., 2018). These changes have been observed across snow-dominated regions globally, including the western United States, Europe, and High Mountain Asia, where shifts in snow accumulation and melt timing directly influence water availability and ecosystem processes. These changes are especially consequential in the western United States, where up to 70% of annual water supply originates as snowmelt (Barnett et al., 2005; Li et al., 2017).

In the western United States, April 1 SWE has declined by 10–30% since the mid-20th century, with the largest declines occurring at lower elevations and in warmer regions (Figure 1; Mote et al., 2018). In Colorado's Rocky Mountains, peak SWE has shifted earlier by approximately 1–2 weeks since the 1980s, with corresponding advances in SDD (Clow, 2010). More recent analyses continue to show widespread shifts toward earlier peak SWE and melt timing, along with increasing variability in snowpack persistence across the western U.S. (Hale et al., 2023). As a result, earlier runoff can disrupt the seasonal alignment between water supply and demand.

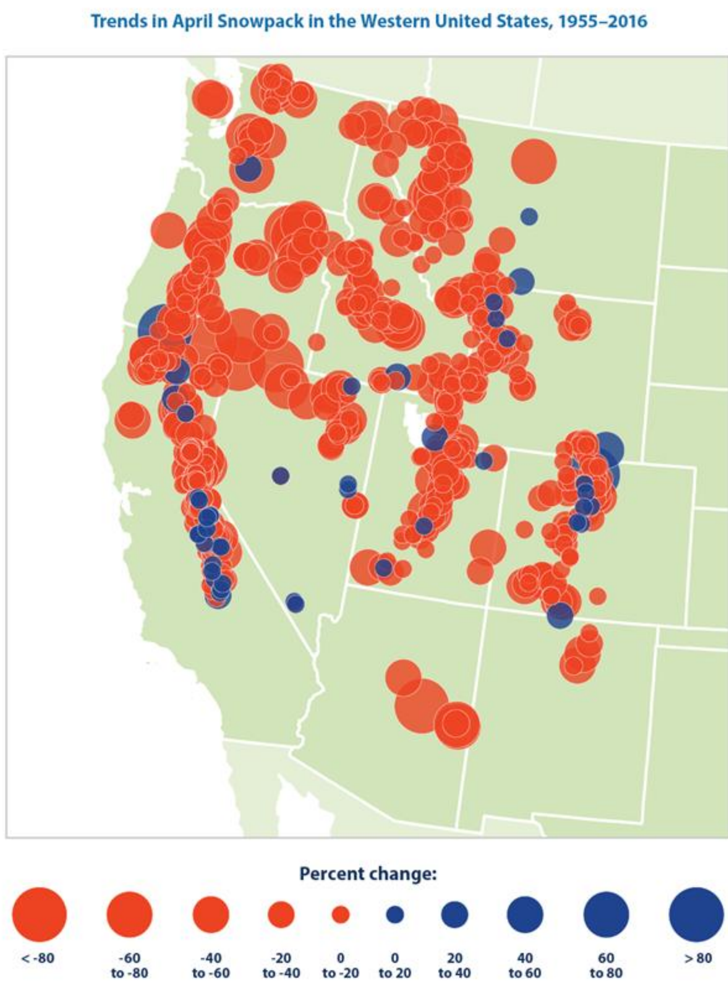

Figure 1. Long-term trends in April 1 snow water equivalent (SWE) across the western United States, showing widespread declines in snowpack (U.S. EPA, 2016, based on Mote et al., 2005).

1.2. Snow Energy Balance and Spatial Heterogeneity

Snowpack evolution is governed by the snow energy balance, including shortwave and longwave radiation, sensible and latent heat fluxes, and ground heat exchange (Marks et al., 1999). Among these components, net shortwave radiation, or solar energy absorbed by the snowpack, is often the dominant energy source during the ablation season (Marks and Dozier, 1992). Snow albedo is therefore a key control on absorbed energy and the rate of snowmelt (Painter et al., 2012; Skiles et al., 2018).

Snow accumulation and melt are highly heterogeneous across mountainous terrain due to variability in topography, vegetation, and orographic effects on atmospheric forcing. Elevation gradients control air temperature and precipitation phase (rain, snow, or mixed), while slope and aspect of the terrain control the magnitude and timing of shortwave radiation reaching the ground surface (Pomeroy et al., 1998). Wind redistribution can further modify the spatial distribution of snow through preferential deposition and erosion, which can result in substantial variability in snow depth and SWE across short distances in a watershed (Dyunin and Kotlyakov, 1980; Liston and Sturm, 1998; Sexstone et al., 2018). Vegetation introduces additional complexities to snow distribution and melt processes through canopy interception of snowfall, altering turbulent fluxes, and emitting longwave radiation (Pomeroy et al., 1998). These interacting controls make snowpack evolution difficult to capture through point observations alone, and models must account for these interactions to accurately represent snow processes.

1.2.1. Changes in Snow Albedo

In the western United States, increased frequency and magnitude of dust deposition on snow events over recent decades have led to measurable reductions in snow albedo and earlier snowmelt timing (Painter et al., 2007; Painter et al., 2012; Skiles et al., 2018). Deposition of dust and other light-absorbing impurities lowers snow albedo, enhancing shortwave radiation absorption and accelerating snow grain size growth, further reducing albedo through positive feedback. These effects are amplified as the snowpack evolves and impurity concentrations increase at the snow surface during ablation, ultimately advancing SDD by several weeks and altering the timing and magnitude of runoff in snow-dominated watersheds (Skiles et al., 2018). These processes provide a useful analog for post-fire environments, where deposition of charred organic material similarly reduces snow albedo and alters melt dynamics.

1.3. Snow Observation Techniques for Water Resources Management

Snowpack accumulation and melt patterns are routinely monitored and modeled by water resource agencies to inform water supply forecasting and management decisions (Barnett et al., 2005). Snowpack conditions are observed through a combination of ground-based measurements and remote sensing products, each providing complementary insights across spatial and temporal scales. In situ observation networks, including Snow Telemetry (SNOTEL) stations, provide long-term records of SWE, snow depth, and meteorological data (i.e., air temperature, wind speed, precipitation), and are the basis for operational water supply forecasting in the western United States (Serreze et al., 1999). These measurements offer high temporal resolution but are limited to point-scale spatial observations and may not capture spatial variability across complex mountain terrain.

Remote sensing approaches provide spatially distributed observations of snowpack across scales that cannot be captured by point measurements alone. Optical sensors such as MODIS and VIIRS provide spatially distributed estimates of snow cover extent and albedo, while airborne techniques such as the Airborne Snow Observatory (ASO) provide high-resolution lidar measurements of snow depth over a watershed (Hall and Riggs, 2007; Painter et al., 2016;

Palomaki et al., 2025). Active microwave remote sensing approaches further expand these capabilities by enabling observations that are independent of cloud cover and solar illumination influences (Ulaby et al., 1986). Synthetic aperture radar (SAR) sensors, such as Sentinel-1, have been used to estimate snow properties through backscatter-based methods and interferometric synthetic aperture radar (InSAR) techniques, which are also sensitive to changes in liquid water content within the snowpack, enabling detection of melt onset (Nagler et al., 2016; Gagliano et al., 2023). Emerging L-band SAR systems, including airborne UAVSAR and the recent launch of the NISAR satellite, show strong potential for improving large-scale SWE estimation and snow monitoring (Bonnell et al., 2025). As a result, integrating ground observations and remotely sensed snow observing technologies is a key approach in snow hydrology.

1.4. Snow-Wildfire Interactions

1.4.1. Western U.S. Wildfire Activity

Snow-wildfire interactions are increasingly relevant as wildfire frequency, size, and severity continue to rise in a warming climate (Abatzoglou and Williams, 2016; Iglesias et al., 2022; Kampf et al., 2022; Parks and Abatzoglou, 2020; Westerling, 2016). Across the western United States, increases in wildfire activity have been linked to earlier snowmelt, longer dry seasons, and more arid climatic conditions, which together promote longer wildfire seasons and more favorable conditions for large, high-severity fires (Westerling, 2016; Abatzoglou and Williams, 2016). In addition to climatic drivers, land management practices and historical fire suppression have contributed to increased fuel loads in many forested systems (Parks and Abatzoglou, 2020; Stevens-Rumann and Morgan, 2019). As a result, large, high-severity wildfires are becoming more common in snow-dominated headwater regions, increasing the likelihood of wildfires impacting seasonal snowpack (Figure 2; Kampf et al., 2022). Recent work has shown that 70%

of seasonal snow zones have experienced increases in wildfire area since 1984, and in 2020 alone the Southern Rockies saw more total area burned in the seasonal snow zone than the previous 36 years combined (Figure 2; Kampf et al., 2022).

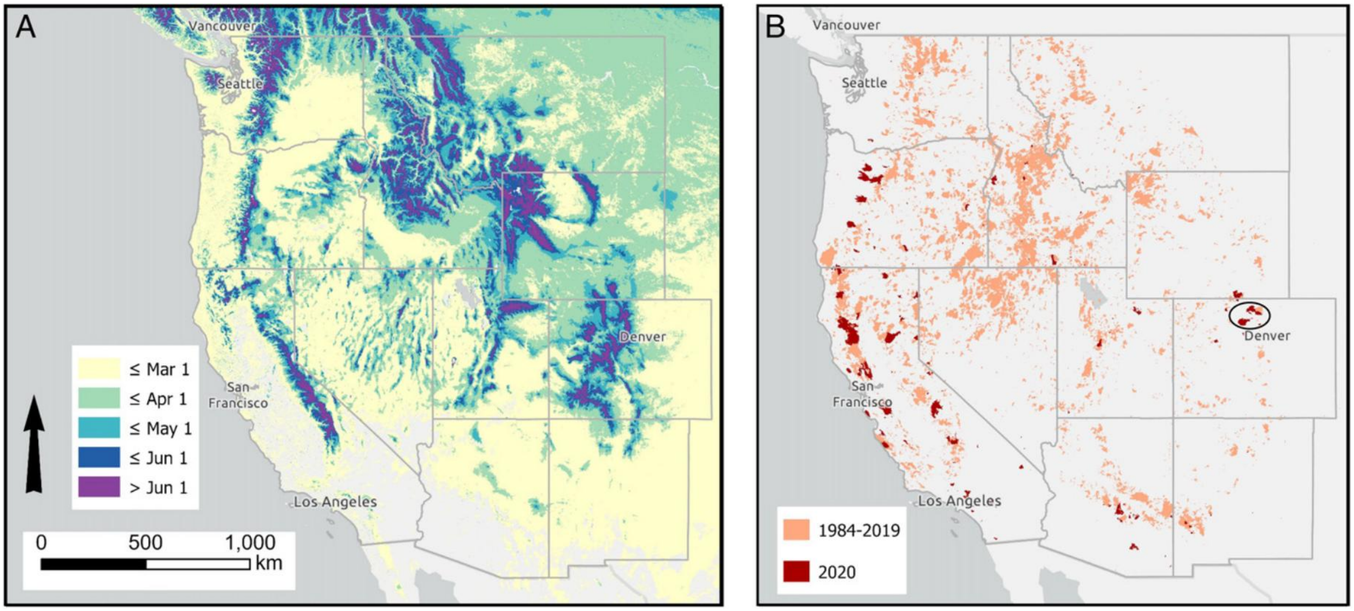

Figure 2. Snow zones (A) and historical fire boundaries (B) in the western United States. Colorado's 2020 Cameron Peak and East Troublesome Fires are circled. Figure from Kampf et al., 2022.

1.4.2. Canopy Loss and Vegetation Changes

In unburned forests with intact canopy structures, canopy interception of snowfall can result in sublimation losses, though canopy shading reduces incoming shortwave radiation which can delay the onset of melt (Pomeroy and Gray, 1995; Hedstrom and Pomeroy, 1998). These competing mechanisms result in lower snowfall accumulation in forests compared to open meadow landscapes, but longer snowpack persistence.

Wildfires often result in the loss of forest canopy, which reduces interception of snowfall and increases snow accumulation on the ground surface (Burles and Boon, 2011). The loss of forest canopy exposes the snowpack to greater shortwave radiation, accelerating snowmelt (Schwartz et al., 2020; Reis et al., 2024). The relative impact of these mechanisms in burned forests depends on the burn severity, remaining canopy structure, and snow climate regime (Koshkin et al., 2022). Despite snow accumulation increases in burned forests due to the loss of canopy interception, increases in shortwave radiation reaching the snowpack following canopy loss result in accelerated melt and earlier snow disappearance compared to unburned forests (Reis et al., 2024). These changes can persist for years to decades, and some impacts may be permanent on human time scales through conversion of forest type to open meadow following high-severity fire (Coop et al., 2022; Stevens-Rumann and Morgan, 2019).

1.4.3. Post-Fire Snow Albedo Impacts

Charred debris and soot deposited onto the snow surface can lower snow albedo and thus accelerate melt, leading to earlier snow disappearance (Gleason and Nolin, 2016; McGrath et al., 2023; Burles and Boon, 2011). In burned forests, reductions in snow albedo have been shown to persist for multiple post-fire winters, with the strongest effects occurring during snowmelt when canopy loss and surface impurities act together to enhance radiative forcing (Gleason and Nolin, 2016). Previous work has shown that post-fire reductions in snow albedo are evident 15 years following disturbance (Gleason et al., 2019). As forests recover post-fire, snow albedo has also been shown to gradually increase as the availability of surface impurities from burned biomass declines, though the pace of recovery varies depending on tree density, species composition, and the time since fire (Gleason and Nolin, 2016; Gersh et al., 2022; Surunis and Gleason, 2024; Uecker et al., 2020).

1.4.4. Land Surface Albedo and Remote Sensing of Snow Albedo

These post-fire changes in snow albedo occur alongside broader shifts in land surface albedo, which often increases following wildfire as vegetation loss exposes brighter underlying surfaces, although the magnitude and direction of change can vary with ecosystem type and burn severity

(Gayler and Skiles, 2024; Gersh et al., 2022; Lyons et al., 2008). While snow albedo refers specifically to the reflectivity of the snowpack surface, land surface albedo encompasses the reflectivity of exposed ground, vegetation, and burned debris. This distinction becomes particularly important in post-fire environments, where snow albedo and land surface albedo often show contrasting responses (Figure 3). Snow albedo generally declines due to deposition of light absorbing impurities, whereas land surface albedo may increase following canopy loss as brighter underlying surfaces are exposed and shading is reduced (Figure 3).

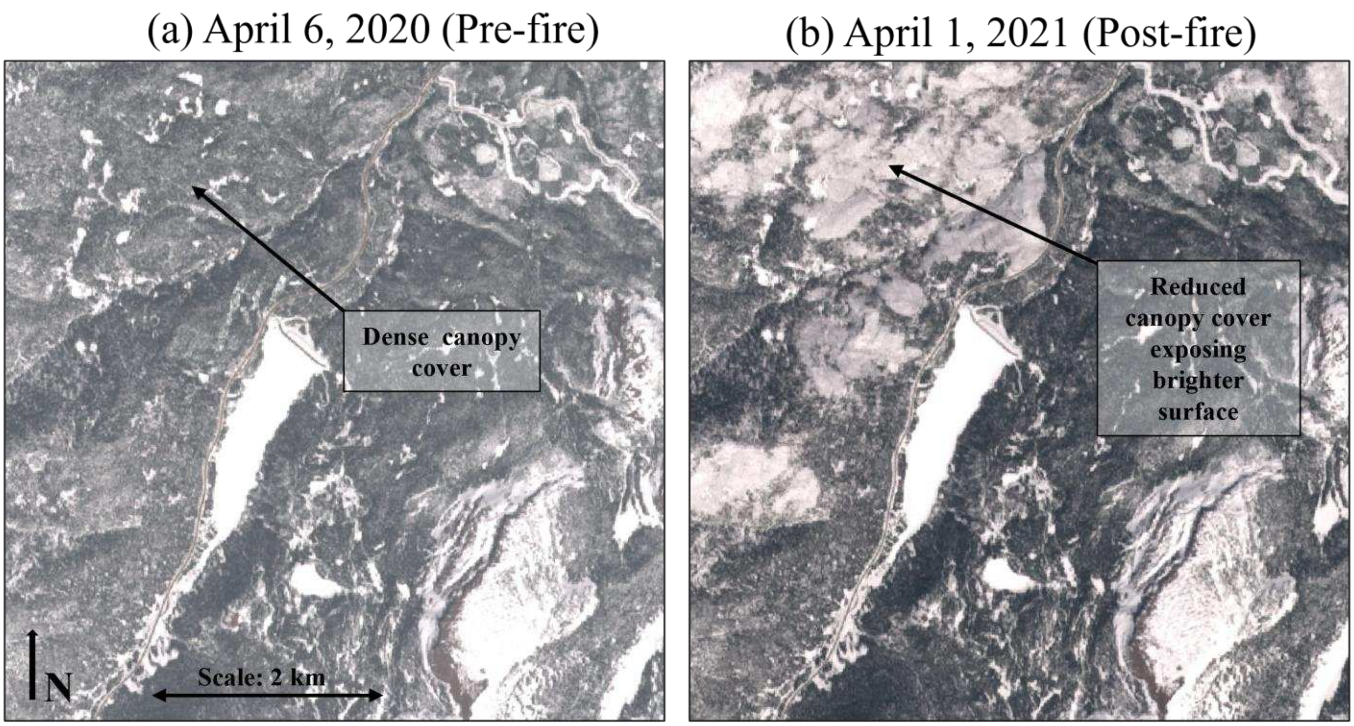

Figure 3. Sentinel-2 imagery of the Cameron Pass study area during spring conditions before (a) and after (b) the 2020 Cameron Peak Fire, showing the exposed snow surface following removal of the forest canopy.

Observing these dynamics requires multiple approaches: ground-based stations capture high-frequency, point-scale measurements of snow albedo under consistent geometry, while satellite products (e.g., MODIS and VIIRS) offer spatially extensive estimates that integrate both snow and land surface contributions (Hall and Riggs, 2007; Schaaf et al., 2002; Wang et al., 2018; Key et al., 2013). Recent advances in snow albedo retrievals using spectral unmixing and fractional snow-covered area have improved representation of snow properties in heterogeneous terrain (Rittger et al., 2020; Palomaki et al., 2025). However, satellite-derived albedo may not fully capture fine-scale variability in snow surface conditions (Schaaf et al., 2002; Wang et al., 2018), particularly in complex, post-fire environments.

1.5. Influence of Snow Climate Regime

The relative impact of disturbances on snowpack dynamics is further influenced by the regional snow climate regime. Continental snow climates, such as Colorado's Rocky Mountains, are typically characterized by cold, shallow, and more persistent snowpacks (Serreze et al., 1999; Trujillo and Molotch, 2014). In contrast, snowpacks in the Sierra Nevada or Pacific Northwest are often associated with warmer and deeper snowpacks, though their meteorology and storm patterns differ and are not uniformly maritime (Serreze et al., 1999; Trujillo and Molotch, 2014). Intermountain regions typically reflect characteristics that are intermediate between maritime and continental snow climates. These climate regimes are also associated with differences in forest structure, including tree density, canopy height, and spacing, which influence snow accumulation and energy balance through interception and shading (Hedstrom and Pomeroy, 1998; Pomeroy and Gray, 1995). Denser forests typical of maritime regions can enhance canopy shading and interception losses, while more open subalpine forests in continental regions allow more solar radiation to reach the snow surface, amplifying the effects of canopy disturbance.

These differences affect baseline snowpack behavior and the response to disturbances like wildfires. In continental snow climates, clear-sky conditions and high solar radiation during spring have been shown to amplify the effects of light-absorbing impurities on snow (Skiles et al., 2018; Painter et al., 2012), whereas regions with more frequent cloud cover may experience reduced incoming shortwave radiation, which can limit the effects of impurity driven albedo reductions (Trujillo and Molotch, 2014). However, episodic mid-winter dry spells in the Sierra Nevada have been shown to produce long stretches of high pressure, resulting in enhanced shortwave radiation and accelerated melt (Hatchett et al., 2023), highlighting the potential for short term atmospheric variability to influence snow energy balance before the ablation period. As a result, post-fire changes in snowpack dynamics are not uniform across regions, and understanding these dynamics requires consideration of local climatic characteristics.

1.6. Snowpack Modeling in Disturbed Environments

1.6.1. Historical Modeling Challenges

Forest disturbances resulting from wildfires, especially their impacts on snowmelt processes, are challenging to implement in current snow models. Temperature-index models such as SNOW-17 (Anderson, 1976) often rely on empirical relationships between historical air temperature and melt rates to predict the quantity and timing of snowmelt, with parameters adjusted by water forecasters for specific watersheds. As a result, temperature index models are computationally efficient and widely used in operational water forecasting. While parameters in these models can be adjusted to account for increased melt due to disturbances such as wildfires, these approaches do not explicitly represent the underlying processes driving changes in snow energy balance. Additionally, enhanced melt rates are applied to the entire modeling domain, which could include unburned areas that do not experience accelerated melt, limiting their ability to represent spatially heterogenous melt dynamics. In contrast, energy balance models simulate individual fluxes that control snowpack evolution, providing a more physically based representation of melt processes. However, these models require accurate climate forcing data and are generally more computationally expensive and challenging to implement.

1.6.2. Implementation of Physically Based Snow Models

iSnobal is a snow energy and mass balance model that can be run in both spatially distributed and point configurations to simulate snow accumulation and melt processes (Marks et al., 1999). iSnobal calculates the surface energy balance, accounting for shortwave and longwave radiation, sensible and latent heat fluxes, ground heat exchange, and phase changes within the snowpack (Havens et al., 2020; Marks et al., 1999). Implementing a physically based model allows for improved representation of post-fire changes in snow processes, including changes in canopy cover and accelerated albedo decay. These processes can be represented through the High-Resolution Rapid Refresh (HRRR) numerical weather prediction model (Benjamin et al., 2016) and revised parameterizations (e.g., albedo decay rates, minimum albedo thresholds). The model has been widely used in research on snow hydrology and climate variability (Garen and Marks, 2005; Marks et al., 2013; Sexstone et al., 2018), offering an improved framework for evaluating snowpack evolution in complex terrain.

1.6.3 Uncertainties in Post-Fire Snow Energy Balance Modeling

Despite these advantages of physically based models, uncertainties remain in their ability to represent changes in disturbed environments. Accurate modeling of snowpack dynamics requires high-quality meteorological forcing data, including incoming shortwave radiation, air temperature, humidity, and wind speed and direction, which are difficult to observe and predict at high-resolution in complex mountainous terrain (Havens et al., 2020; Meyer et al., 2023). Errors in meteorological forcing data propagate into snow energy balance calculations and simulated snow accumulation patterns, which influence melt rates and the overall timing of snow disappearance. Additionally, parameterizations of snow processes such as snow albedo evolution, canopy interception, and turbulent fluxes are often simplified in snow models compared to highly variable natural systems (Clark et al., 2011). In post-fire environments, these challenges are amplified by substantial changes in vegetation structure, snow surface properties, and increased inputs of light absorbing impurities from charred plant material, which standard model configurations do not fully capture (Gleason and Nolin, 2016; Gayler and Skiles, 2024). As a result, improving representation of post-fire impacts in snow energy balance models remains a significant area of research, especially as wildfire activity continues to increase in seasonal-snow zones (Kampf et al., 2022).

1.6.4 Post-Fire Snow Albedo Modeling

Post-fire snow albedo evolution presents a critical source of uncertainty in snow energy balance modeling (Gleason and Nolin, 2016; Skiles et al., 2018; Gayler and Skiles, 2024). Traditional albedo parameterizations are often based on time since snowfall or empirical decay functions (Marshall and Warren, 1987; Marks and Dozier, 1992; Essery et al., 2013), which do not account for the effects of increased inputs of light-absorbing impurities on snow albedo evolution. In burned environments, deposition of charred debris accelerates snow albedo decay, resulting in more rapid darkening of the snow surface following snowfall events compared to standard model representations (Gleason and Nolin, 2016). Accurately capturing these dynamics requires observation-constrained parameterizations that reflect snow albedo decay conditions in post-fire environments, especially as these altered conditions vary with time since fire. Integrating in situ observations of albedo decay into model frameworks therefore provides a pathway for improving representation of post-fire processes in snow energy balance models.

1.7. Study Overview and Objectives

This study integrates established field-based observations and emerging snow observing technologies to examine spatial and temporal patterns in albedo dynamics in wildfire-impacted seasonal snow zones and their implications for snow energy balance modeling. By integrating in situ observations with the physically based iSnobal model, this study incorporates observation-informed parameterizations to improve representation of post-fire albedo evolution. In situ observations include continuous measurements of snow albedo, snow depth, and meteorological conditions following five post-fire winters, which provides high-temporal resolution observations necessary for parameterizing post-fire snowpack dynamics. The selected study site, located within the Cameron Peak wildfire area in north-central Colorado, provides an ideal study area to leverage ongoing observations of post-fire snow energy balance, albedo dynamics, and vegetation recovery. Comparing iSnobal simulations to ground-based measurements provides a direct evaluation of the model's ability to capture post-fire changes in snowpack evolution and improve understanding of snow water resources in disturbed landscapes.

The objectives of this study are to (1) quantify event-scale snow albedo decay and ablation-season albedo recovery in a burned forest environment across five post-fire winters (2021–2025), including characterization of variability in decay rates relative to the snowpack conditions and timing within the melt season, (2) integrate field-derived albedo decay parameterizations into iSnobal and evaluate agreement with observations of snow disappearance timing, melt rates, and surface energy balance in fire-impacted basins, and (3) assess the relative importance of post-fire albedo change versus canopy loss in controlling snowpack energy balance and melt dynamics.

2. STUDY AREA

The Cameron Pass study area (Figure 4), situated in north-central Colorado within the headwaters of the Cache la Poudre River, is a high-elevation, snow-dominated region that supplies water for downstream communities along Colorado's Front Range. This area was heavily impacted by the Cameron Peak Fire, the largest wildfire in Colorado history, which burned over 840 km^2 from August to December 2020. This fire spanned a broad elevation gradient (~1,600 to ~3,400 m), including large areas of moderate to high burn severity, resulting in substantial loss of forest canopy and widespread deposition of charred material across the landscape (Coop et al., 2022; McGrath et al., 2023; Reis et al., 2024).

Seasonal snowpack persistence varies strongly with elevation across this study area, with a consistent, persistent snowpack typically developing above ~2,500 m and significant increases in depth at higher elevations. The nearby Joe Wright SNOTEL station (3,080 m) has an average peak SWE of approximately 615 mm, and snow cover typically persists from mid to late-October through mid-June, reflecting a cold, continental snow climate. Vegetation in the study area is dominated by subalpine conifer forests, including lodgepole pine (Pinus contorta), Engelmann spruce (Picea engelmannii), and subalpine fir (Abies lasiocarpa). Cameron Pass offers a unique opportunity to study post-wildfire snow processes in a high-elevation environment where seasonal snowpack plays a critical role in regional water resources (Kampf et al., 2022; Li et al., 2017).

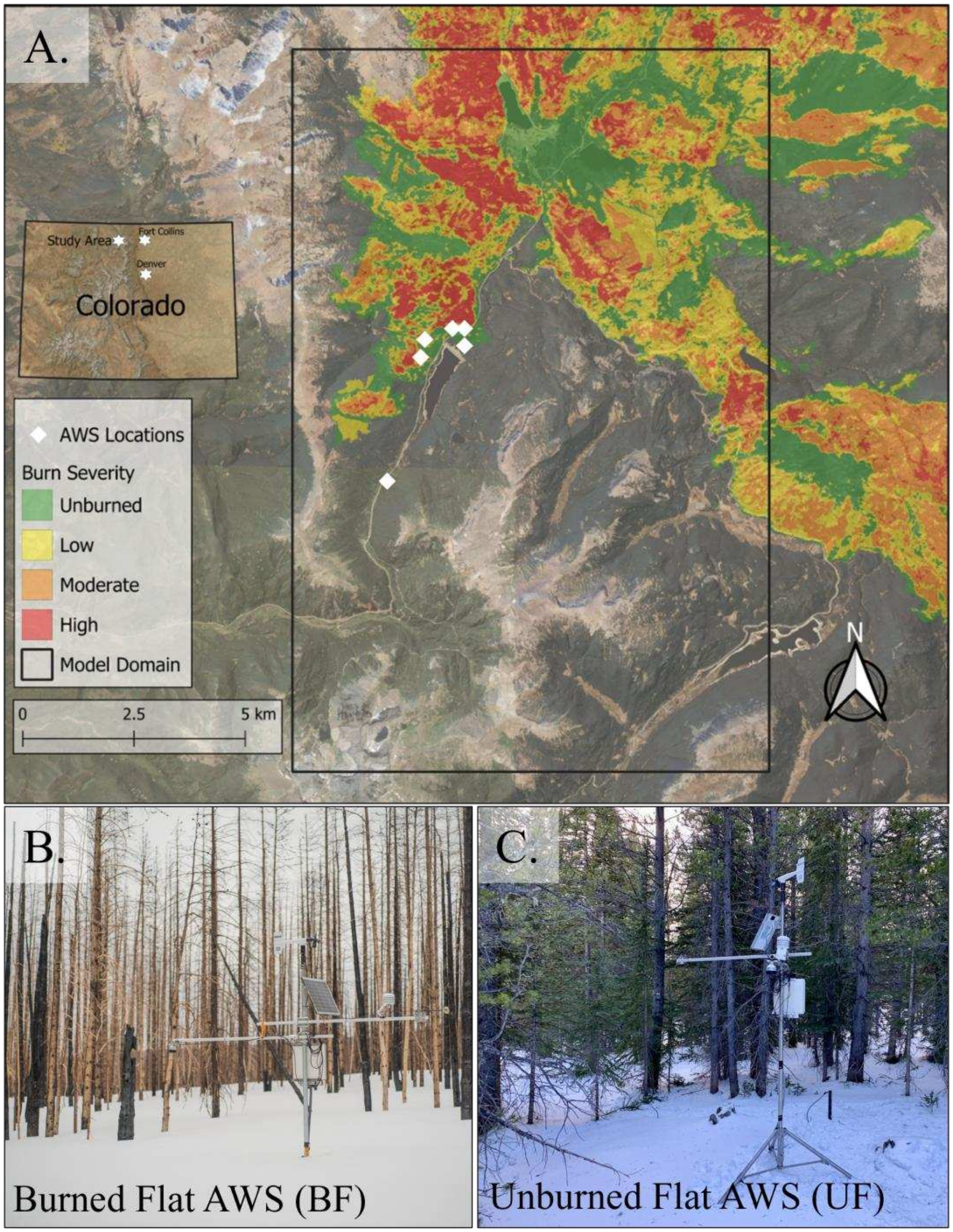

Figure 4. Map of the Cameron Peak Fire study area showing Burned Area Emergency Response (MTBS) burn severity and the iSnobal model domain. White symbols indicate the locations of automatic weather stations (AWS), and the black rectangle outlines the model domain. (B) Site photos from the Burned Flat (April 2024) and (C) Unburned Flat AWS (November 2021) locations.

3. DATA AND METHODS

3.1 Instrumentation

Observations from five automatic weather stations (AWS) were used to capture snowpack and energy balance processes across burned and unburned sites within the study area. Stations were strategically placed to capture variability in burn conditions, aspect, and slope.

Incoming and reflected shortwave radiation were measured at Burned Flat and Unburned Flat AWS using Apogee Instruments SN-500-SS pyranometers (upward-looking sensor: 385–2105 nm; downward-looking sensor: 370–2240 nm), while the remaining sites used Kipp and Zonen CNR1 radiometers with CM3 pyranometers (305–2800 nm). Albedo was calculated as the ratio of reflected (outgoing) to incoming shortwave radiation.

Hourly measurements of snow depth (Campbell Scientific SR-50), air temperature (Campbell Scientific HygroVUE10), relative humidity, and wind speed (Campbell Scientific/ RM Young 05108) were also collected. Station metadata, including location, elevation, burn classification, and period of record, are provided in Table 1. Data availability spans water years (WY) 2021–2025 but is site-dependent.

In addition to these AWS stations, this study uses data from the Joe Wright SNOTEL station, a long-term Natural Resources Conservation Service (NRCS) snow monitoring site located within the study area. The Joe Wright SNOTEL site provides continuous measurements of SWE, precipitation, and air temperature (Serreze et al., 1999; Clow et al., 2010).

Table 1. Site information for Automatic Weather Stations used in this study and the Joe Wright SNOTEL station. Topographic parameters are from UAV-lidar derived 1 m digital elevation models (DEMs). Burn severity information is from the Monitoring Trends in Burn Severity (MTBS) dataset. Coordinates are referenced to the WGS 84 / UTM zone 13N coordinate reference system (EPSG: 32613).

Site Name	Installation Date (Month – Year)	Latitude°	Longitude°	Elevation (m)	Slope °	Aspect °	Burn Severity (MTBS)
Burned Flat	Jan–21	40.563	-105.867	3009	2.1	65	High
Burned North	Oct–22	40.561	-105.877	3095	8.7	40	High
Burned South	Oct–22	40.557	-105.879	3102	17.1	220	High
Unburned Flat	Nov–21	40.563	-105.870	3019	5.6	170	–
Unburned North	Oct–22	40.560	-105.867	2991	6.9	15	–
Joe Wright SNOTEL	Oct–78	40.532	-105.887	3091	4.0	315	–

3.2 Field Observations

Field observations were collected 1–2 times per month each winter during the study period (WY 2021–2025). Snow pit measurements of bulk density were collected within 20 m of each AWS station (Table 1) and were used to estimate snow water equivalent (SWE). Snow pits were excavated with the pit wall oriented north and shaded during sampling to minimize the influence of solar radiation. Successive pits were excavated ~1 m behind the previous pit wall during each survey to minimize disturbance from prior measurements. Density observations were performed using the standard wedge cutter technique by extracting 1 L samples from each snow pit face at 10 cm intervals and weighing them to determine density. Two density measurements were taken at each interval, with a third measurement collected if the first two differed by more than 10%. Bulk snow density was calculated from these measurements.

To construct a continuous daily SWE time series, daily sonic-derived snow depth observations were combined with a snow density time-series. The density time-series was constructed by first finding the difference between the snow pit observations at each site and the Joe Wright SNOTEL density on each observation date and linearly interpolating these differences. This site-specific daily difference was then applied to the Joe Wright station density to produce a site-specific density time series that captured the day-to-day variability in density as measured by the SNOTEL station with the absolute magnitude of the snow pit measurements. Additional in situ observations include manual snow depth probing and camera-derived snow stake measurements of snow depth across the study area.

UAV lidar surveys were conducted approximately monthly during the snow-covered season using a DJI Matrice 350 RTK UAV equipped with a Zenmuse L2 lidar sensor. Flights covered an approximately 1 km^2 area and were flown at ~60 m above ground level (AGL) yielding a point cloud density of ~400 pts/m^2. The surveys were processed and classified using DJI Terra software and then gridded to produce 1 m resolution digital elevation models (DEMs).

3.3 Slope and Aspect Correction

Observed broadband snow albedo measurements from AWS stations were corrected for terrain effects from slope and aspect following the methodology outlined in Painter et al. (2012). The corrected albedo was computed as:

$$\boldsymbol{\alpha_{corr}} = \boldsymbol{\alpha_{obs}} \left(\frac{\boldsymbol{cos\theta_s}}{\boldsymbol{cos\theta_i}}\right) \tag{1}$$

Where $\boldsymbol{\alpha_{obs}}$ is the AWS measured albedo on a sloped surface, $\boldsymbol{\alpha_{corr}}$ is the corrected albedo representing the equivalent albedo referenced to a horizontal surface, $\boldsymbol{\theta_s}$ is the solar zenith angle, and $\boldsymbol{\theta_i}$ is the solar incidence angle relative to the sloped surface. The solar incidence angle was computed as:

$$\boldsymbol{cos\theta_i = cos\theta_s cos\beta + sin\theta_s\, sin\beta}\ \mathbf{cos}\,\{\boldsymbol{\gamma_s - \phi}\} \tag{2}$$

where $\boldsymbol{\beta}$ is the slope angle, $\boldsymbol{\phi}$ is the slope aspect, and $\boldsymbol{\gamma_s}$ is the solar azimuth angle.

As the snow surface slope can differ modestly from the ground surface slope, the slope angle and aspect were calculated at each AWS pyranometer sensor location using the median values derived from eight snow-on digital elevation models (DEMs) with UAV lidar at 1 m spatial resolution from WY 2025. To account for small scale topographic variability, median slope and aspect were calculated within a 1 m radius buffer surrounding each AWS location.

To minimize the influence of low solar angles and transient shading effects, daily median albedo values were calculated using measurements collected between 11:00 and 14:00 MST, when solar elevation is highest. Outgoing and net shortwave radiation were adjusted using the slope and aspect corrected albedo measurements.

3.4. Albedo Decay Events

Albedo decay events were defined as periods with at least three consecutive days without new snow following a snowfall event of at least 3 cm. This threshold was selected to capture meaningful snow surface albedo resets while minimizing noise associated with trace precipitation events and is consistent with the methodology outlined by Gleason et al. (2016).

For each decay event, an exponential regression was applied to daily median albedo values ($\boldsymbol{\alpha}$) as a function of days since the last snowfall (t).

$$\boldsymbol{\alpha(t) = \alpha_0\, e^{kt}} \tag{3}$$

The exponential coefficient derived from the fitted regression, $\boldsymbol{k}$, represents the albedo decay rate for an individual event and $\boldsymbol{\alpha_0}$ is the initial snow albedo at the start of a decay event. Decay rates were estimated separately for burned and unburned AWS stations and evaluated across multiple post-fire winters (4 years for unburned stations, 5 years for burned stations).

Several quality control criteria were applied to each identified decay event. Individual events were verified using time-lapse camera imagery to confirm correct identification of snowfall and to account for potential sensor noise (e.g. snow-covered sensor). Each decay event was assigned a quality score ranging from 1 to 3 based on the overall quality of the exponential fit and confidence in the resulting decay coefficient. Events classified as 3 (high quality) exhibited strong exponential behavior (high R^2, typically >0.7) and clear correspondence with time-lapse–confirmed snowfall and decay behavior. Score 2 (moderate quality) events showed reasonable exponential structure (moderate R^2, ~0.4–0.7) with minor uncertainty in event timing or short periods of sensor noise but exhibited physically consistent exponential decay. Score 1 (low quality) events exhibited poor exponential fit (low R^2, <0.4), ambiguous snowfall timing, or substantial sensor contamination and were excluded from analysis. Only events with quality scores of 2 or 3 were retained for subsequent analysis.

For subsequent modeling parameterizations, ablation season decay rates were only selected after 15 March. This date was selected to provide a direct comparison with the base iSnobal configuration, further described in section 3.6.1. An example of the exponential regression fit is included in Supplementary Figure 1, and the full dataset of all decay events is provided in the associated data repository.

Controls on albedo decay were evaluated using event-scale metrics derived from AWS observations. For each valid decay event, variables including timing relative to peak SWE, prior albedo before snowfall reset, and snowfall magnitude were quantified. These metrics were used to characterize variability in decay behavior across burned conditions and water years.

3.5. Albedo Recovery Assessment

Post-fire albedo recovery was quantified using seasonal minimum and median albedo metrics from the burned flat AWS station from 15 April to SDD, excluding periods influenced by new snowfall. Interannual trends were evaluated to characterize post-fire recovery trajectories. Burned sites were analyzed independently to evaluate variability in recovery behavior; unburned sites were excluded due to persistent canopy shading effects that substantially reduce comparability with open, post-fire conditions. In addition, albedo decay rates were examined across successive winters to assess longer-term trends in decay behavior during post-fire recovery.

3.6. iSnobal Model Runs

The iSnobal snow energy and mass balance model, implemented here through the Automated Water Supply Model (AWSM; Havens et al., 2020), was used to simulate snow accumulation and melt processes across the Cameron Peak Fire study area. The model domain consists of a 174 km^2 area covering an elevation gradient of 2,633 to 3,839 m and was run at 30 m resolution with hourly time steps. The required meteorological forcing data for all model runs were from the NOAA High Resolution Rapid Refresh (HRRR) numerical weather prediction model at 3 km resolution and were spatially distributed across the model domain using terrain-based adjustments from the Spatial Modeling for Resource Framework (SMRF; Havens et al., 2022). iSnobal model components are publicly available through the community GitHub repository (https://github.com/iSnobal) and model setup and configuration are further described in Meyer et al. (2023).

3.6.1. iSnobal Base Model Configuration

A default model configuration was executed to serve as a control for evaluating post-fire modifications to model physics. In the standard configuration, snow albedo decays according to a time-based decay formulation, with an additional period of accelerated decay following a user-configurable date. This date is typically set based on regional and basin-specific conditions. Albedo decay is controlled by modeled snow grain size growth and solar geometry, represented as a function of time since last snowfall. Grain size is modeled with changes in visible (280–700 nm) and infrared (700–2800 nm) albedo using empirically derived relationships following Marshall and Warren (1987) and Marks and Dozier (1992). iSnobal broadband albedo was computed using a ratio of 54% visible wavelength albedo and 46% infrared albedo.

The base albedo implementation accounts for the influence of solar geometry through a cosine-of-zenith-angle correction, allowing albedo to vary diurnally as a function of sun angle (Marks and Dozier, 1992). For periods when the sun is above the horizon, both visible and infrared albedo are adjusted based on the deviation of the local solar zenith angle from overhead illumination. The reset albedo following a storm event during accelerated decay is determined by time since the last storm and albedo evolution is calculated independently for each model grid cell.

3.6.2. Post-Fire Albedo Parameterization and Exponential Decay Model

A post-fire modified albedo decay option was implemented in the model and can be activated via a user-defined parameter in the AWSM configuration file (Meyer et al., 2026). In this configuration, burned and unburned areas within the model domain were delineated using a binary burn mask derived from the Monitoring Trends in Burn Severity (MTBS) dataset, a Landsat-based wildfire severity mapping product for the United States (Eidenshink et al., 2007).

For the binary burn mask, both high and moderate burn severity pixels were assigned a value of 1 and unburned pixels and low burn severity a value of 0.

Following snowfall, albedo is reset using the default model behavior, after which an exponential decay formulation is applied during the ablation period in place of the standard decay function for burned pixels. Although albedo decay rates likely vary across burn severity classes, all available in situ albedo observations from the five AWS stations were located within high burn severity areas. As a result, decay rates were applied uniformly within burned (high and moderate burn severity) and unburned classes.

For each water year, the albedo decay rate implemented in the model was defined as the median event-scale decay coefficient (k) derived from observed exponential fits between 15 March and SDD. This approach provided a single representative ablation-season decay rate for each water year. Areas classified as unburned pixels were left unchanged with the default base run albedo configuration.

3.6.3. LANDFIRE Modification and Combined Model Configuration

To evaluate the relative impact of canopy loss versus snow albedo modifications on post-fire snow dynamics, additional model experiments were conducted using updated land cover parameterizations derived from post-fire LANDFIRE (LF) datasets (Rollins, 2009). The base model configuration represents pre-fire vegetation conditions, whereas the LF configuration incorporates time-varying vegetation type and height to reflect wildfire-driven changes in canopy structure.

Updated LF vegetation classifications were used to modify vegetation parameters within the iSnobal model domain at Cameron Pass following the methodology described in Flynn et al. (in review). The modified parameters included vegetation height, the canopy emissivity coefficient, k, and the canopy transmissivity to diffuse radiation, τ, defined by Link and Marks (1999). These parameters control the amount of radiation emitted from and transmitted through the forest canopy.

To isolate the role of albedo processes, a combined model configuration was implemented that applied the LF-modified vegetation parameters together with the field-derived exponential albedo parameterization developed in this study. Comparisons among the base, LF-modified, and combined configurations provide a framework for assessing the relative contributions of canopy change and albedo evolution to post-fire snowpack energy balance and melt dynamics.

3.7. Model Evaluation Metrics

Model outputs for snow depth, SWE, net shortwave radiation, and broadband albedo were extracted for the point locations of the AWS stations as a continuous hourly time series and compared directly to in-situ observations to evaluate performance under base, LF-modified, and combined configurations.

Modeled SWE time series were compared to observed SWE derived from field-based density measurements combined with station snow depth observations. SDD was defined here as the first date when SWE decreased below a near-zero threshold (< 1 mm) following peak SWE. Differences between modeled and observed SDD were calculated to quantify improvements in melt timing representation under the exponential configuration.

Cumulative distribution functions (CDFs) of daily albedo values between peak SWE and SDD were calculated for observations and model runs to characterize the distribution and temporal persistence of albedo conditions during the ablation season. Kolmogorov–Smirnov (KS) statistics (Massey, 1951) were then computed to quantify differences between modeled and observed albedo distributions.

Snowmelt dynamics were evaluated using daily SWE change (ΔSWE). Daily melt rates were computed as the positive component of −ΔSWE and analyzed over two time windows: (1) from peak SWE to SDD and (2) during manually identified periods of sustained melt. Sustained melt periods were defined for each water year as intervals following peak SWE with consistent daily declining SWE and no new snowfall. Because modeled melt timing differed from observations, sustained melt windows were selected separately for AWS and model runs. The exponential and base configurations used the same sustained melt window for a direct comparison. Melt rate distributions were evaluated to compare the magnitude and variability of modeled and observed snowmelt across water years. This approach enables assessment of whether the exponential albedo formulation improves representation of melt dynamics in burned terrain.

To evaluate surface energy balance representation, cumulative net shortwave energy at the snow surface was calculated over the full snow-covered period. Net shortwave radiation (W m^{-2}) was integrated over time using the model time step and converted to energy units (MJ m^{-2}) by multiplying by the time interval (s) and dividing by 10^6. For hourly model output, this corresponds to:

$$E = \sum(SW_{net} \cdot \Delta t)/10^6 \tag{4}$$

Because albedo directly governs shortwave radiation absorption, agreement in cumulative net shortwave energy provides a process-based metric for assessing whether the modified albedo parameterization improves modeled energy input.

4. RESULTS

4.1. Melt Season Albedo and Post-Fire Recovery

Ablation season albedo metrics (minimum and median daily albedo from 15 April to SDD, without new snow) at the Burned Flat AWS station showed clear interannual variability over the five-year post-fire period (WY 2021–2025) (Figure 5). Median ablation-season albedo ranged from 0.38 to 0.59 across the study period, with minimum values ranging from 0.19 to 0.34. The lowest ablation season albedo values occurred during the first two post-fire winters (WY 2021 median: 0.46; WY 2022 median: 0.38), while higher values were observed in later post-fire years, with peak values in WY 2024 (minimum 0.33; median 0.59). Median albedo increased from 0.38 in WY 2022 to 0.53 in WY 2025, representing a recovery of ~40% over the study period, although WY 2025 remained below the peak median albedo observed in WY 2024.

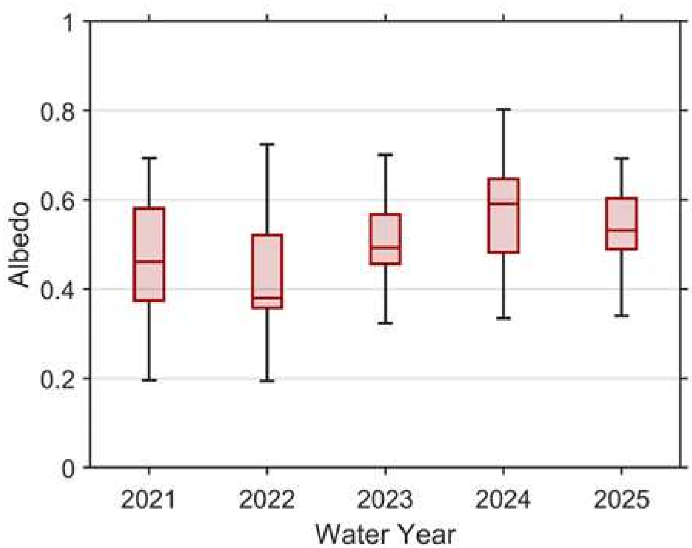

Figure 5. Box plot of daily albedo values in each ablation season (15 April to SDD) during periods without new snow events at the Burned Flat AWS station.

4.2. Albedo Decay Rates

Across WY 2022–2025, burned AWS stations generally exhibited more negative (faster) albedo decay rates following snowfall events compared to unburned sites, although this pattern varied by year (Figure 6). No comparison was available in 2021, as unburned stations were not installed until WY 2022. Median decay rates at burned sites ranged from −0.05 to −0.08 day^{-1}, compared to −0.02 to −0.03 day^{-1} at unburned sites. The largest separation occurred two years post-fire in WY 2022 (−0.08 vs −0.03 day^{-1}) and converged to the smallest difference in WY 2024 (−0.05 vs −0.03 day^{-1}). In WY 2025, median decay rates were similar between burned and unburned sites.

Burned sites also exhibited greater variability in decay behavior, with individual events reaching more negative values (as low as −0.22 day^{-1} in WY 2022), whereas most unburned events ranged between −0.01 and −0.06 day^{-1}, with a single lower outlier of −0.13 day^{-1} in WY 2022.

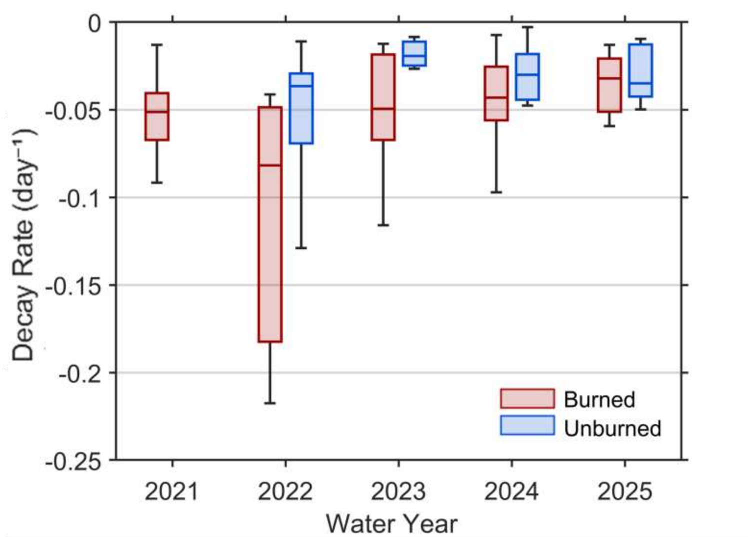

Figure 6. Distribution of albedo decay rate coefficients ($\boldsymbol{k}$) by water year (WY 2021–2025) at burned (red) and unburned (blue) AWS stations. Boxplots show medians, interquartile ranges, and decay coefficients (quality ≥ 2) derived from exponential fits to daily median albedo during identified decay events.

4.3. Controls on Albedo Decay

Linear relationships between albedo decay rate and timing relative to peak SWE were weak for both burned and unburned sites (Figure 7); however, differences in the distribution of decay rates were observed. At burned sites, a greater proportion of decay events occurred after peak SWE (71%) versus unburned events (58%). High-magnitude decay events ($k < -0.10$) were more frequent at burned sites (10% of all events) compared to unburned sites (4% of all events), and 80% of these high-magnitude events at burned sites occurred after peak SWE, whereas no high-magnitude unburned events occurred after peak SWE. Variability in decay rates increased after peak SWE at burned sites (IQR: 0.035 before vs 0.053 day^{-1} after peak SWE), whereas variability at unburned sites remained relatively consistent before and after peak SWE (IQR: 0.030 before vs 0.026 day^{-1} after peak SWE). Differences in the timing of peak SWE between burned and unburned sites may also influence these distributions, as unburned sites generally reached peak SWE later than burned sites.

Decay rates also varied with albedo prior to reset by snowfall events (>3 cm). At burned sites, median decay rates were more negative under lower prior albedo conditions (α <0.60; median: −0.06 day^{-1}) compared to higher prior albedo (α >0.60; median: −0.04 day^{-1}). A weaker contrast was observed at unburned sites (−0.032 vs −0.028 day^{-1}).

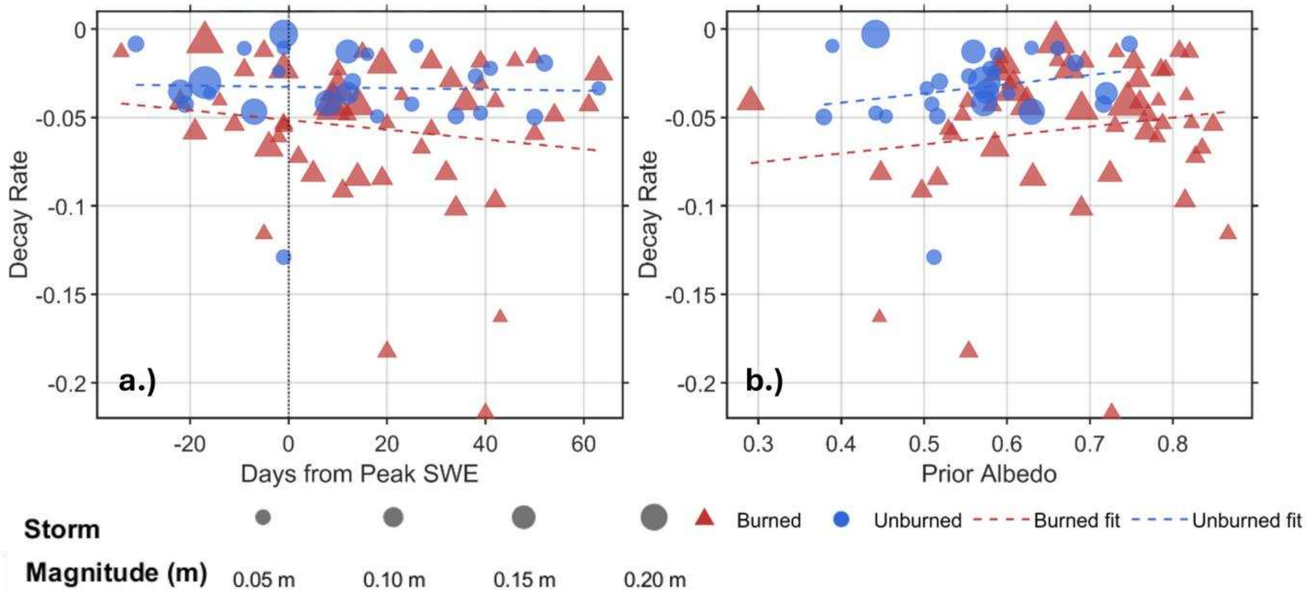

Figure 7. (a) Albedo decay rate as a function of timing relative to peak SWE (days), with the vertical dashed line marking the date of peak SWE. (b) Albedo decay rate as a function of prior albedo for burned (red triangles) and unburned (blue circles) AWS sites across water years 2021–2025. Marker size scales with storm magnitude (m). Solid lines indicate linear fits for each dataset.

4.4. Model Evaluation

4.4.1. SWE and SDD Timing

The base iSnobal configuration consistently predicted later SDD than was observed at the AWS stations, with the largest discrepancies occurring at burned sites (Table 2; Figure 8). At the Burned Flat AWS station (BF), modeled SDD occurred 25–45 days later than observed across water years. Similar late biases were present at the Burned South (BS; 29–51 days) and Burned North (BN; 11–27 days) AWS stations.

Implementation of the exponential albedo parameterization produced earlier SDD at each burned station and water year relative to the base configuration (Table 2; Figure 8). At the Burned Flat AWS station, modeled SDD under the exponential configuration occurred 2–14 days earlier than the base run across water years. Despite this shift, modeled SDD with exponential albedo decay at Burned Flat AWS remained later than observed, with remaining positive biases ranging from approximately 18–31 days relative to AWS observations.

Similar reductions in modeled SDD were observed at the Burned South AWS and Burned North AWS stations. At Burned South, the exponential configuration shifted SDD earlier relative to the base run across all water years (2–16 days). At Burned North, modeled SDD also occurred earlier under the exponential configuration compared to the base configuration (1–13 days). In each water year, SDD simulated using the exponential configuration was closer to observed SDD than the base configuration at burned stations.

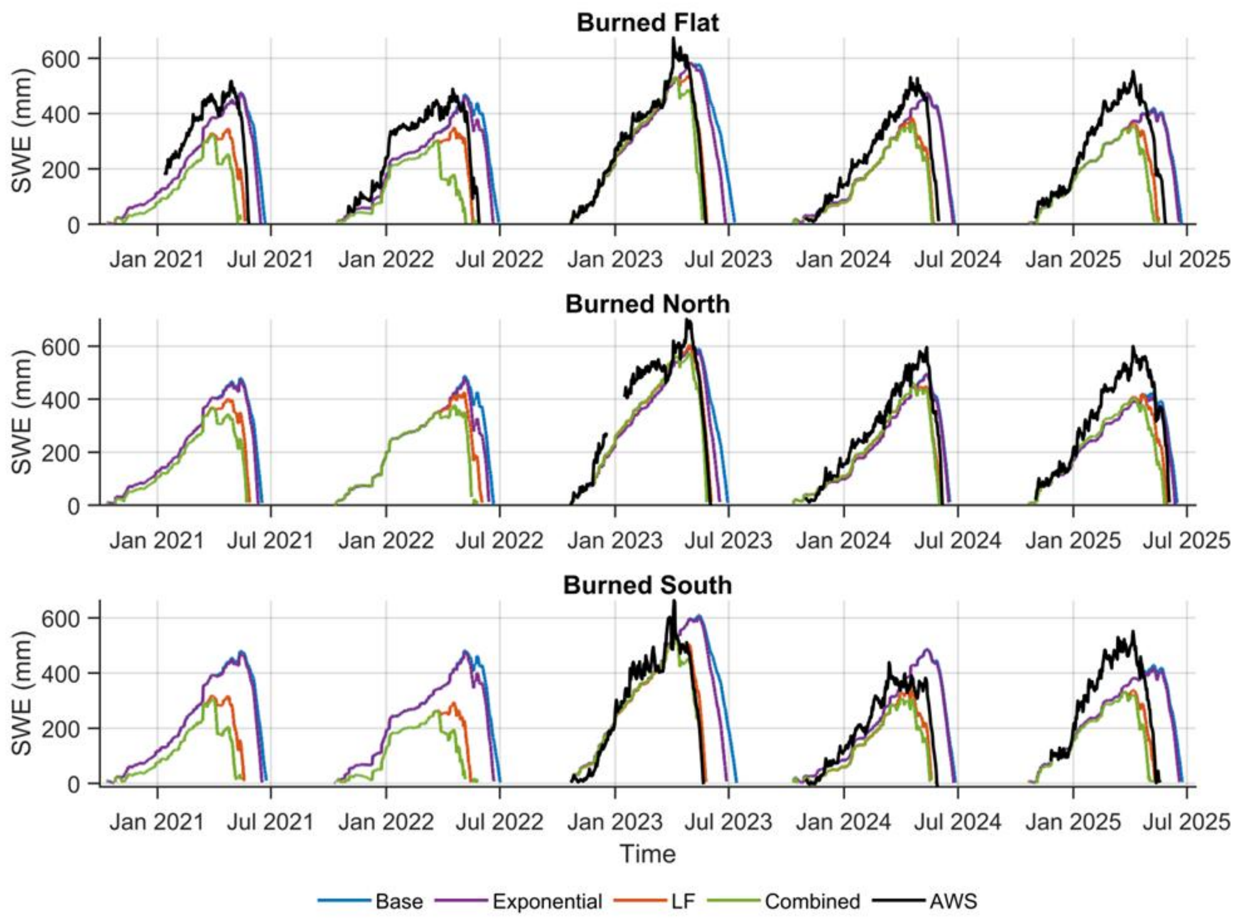

Figure 8. Time series of snow water equivalent (SWE) at the Burned Flat, Burned North, and Burned South AWS sites for water years 2021–2025. Observed SWE from AWS stations (black) is shown with iSnobal model results extracted from each AWS coordinate location for the base model run (blue), exponential (purple), LF (orange), and combined (green).

Table 2. Snow disappearance dates (SDD) and bias relative to AWS observations for burned and unburned sites across water years 2021–2025. Reported values show model-derived SDD in days relative to AWS in parentheses. Positive values (blue) indicate later melt relative to observations, whereas negative values (red) indicate earlier melt. Dates in bold indicate the model run with closest agreement to AWS observations.

Site	WY	AWS	Base	Exponential	Combined	LF
Burned Flat	2021	5/27	06/22 (+26)	06/14 (+18)	05/09 (-18)	**05/20 (-7)**
	2022	5/29	06/29 (+31)	06/20 (+22)	05/07 (-22)	**05/19 (-10)**
	2023	5/26	07/10 (+45)	06/26 (+31)	05/20 (-6)	**05/27 (+1)**
	2024	5/31	06/25 (+25)	06/23 (+23)	**05/20 (-11)**	05/22 (-9)
	2025	5/28	06/22 (+25)	06/18 (+21)	05/09 (-19)	**05/17 (-11)**
Burned South	2023	5/23	07/13 (+51)	06/27 (+35)	**05/21 (-2)**	05/25 (+2)
	2024	5/28	06/26 (+29)	06/24 (+27)	**05/17 (-11)**	05/19 (-9)
	2025	5/13	06/23 (+41)	06/19 (+37)	05/03 (-10)	**05/11 (-2)**
Burned North	2023	6/2	06/29 (+27)	06/16 (+14)	05/27 (-6)	**06/03 (+1)**
	2024	6/6	06/17 (+11)	06/16 (+10)	**06/01 (-5)**	06/02 (-4)
	2025	6/3	06/15 (+12)	06/12 (+9)	**05/26 (-8)**	05/29 (-5)
Unburned Flat	2022	6/13	06/28 (+15)	06/28 (+15)	06/12 (-1)	**06/12 (-1)**
	2023	6/10	07/10 (+30)	07/10 (+30)	**06/17 (+7)**	06/17 (+7)
	2024	6/9	06/24 (+15)	06/24 (+15)	06/07 (-2)	**06/07 (-2)**
	2025	6/8	06/21 (+13)	06/21 (+13)	**06/01 (-7)**	06/01 (-7)
Unburned North	2023	6/26	**06/26 (+0)**	**06/26 (+0)**	06/25 (-1)	06/25 (-1)
	2024	6/22	06/15 (-7)	06/15 (-7)	06/14 (-8)	06/14 (-8)
	2025	6/22	**06/12 (-10)**	**06/12 (-10)**	06/11 (-11)	06/11 (-11)

SDD Bias (days)

-50	-25	0	25	50
Early (-)		Neutral		Late (+)

4.4.2. Modeled versus Observed Albedo

Comparison of modeled albedo from the base configuration with station-measured albedo showed reduced variability in the modeled time series. Modeled albedo values remained above 0.53 throughout the ablation season, whereas station observations exhibited a wider range of albedo values (Figure 9). Observed albedo frequently declined below 0.53 during the ablation period, including sustained periods of lower albedo prior to SDD.

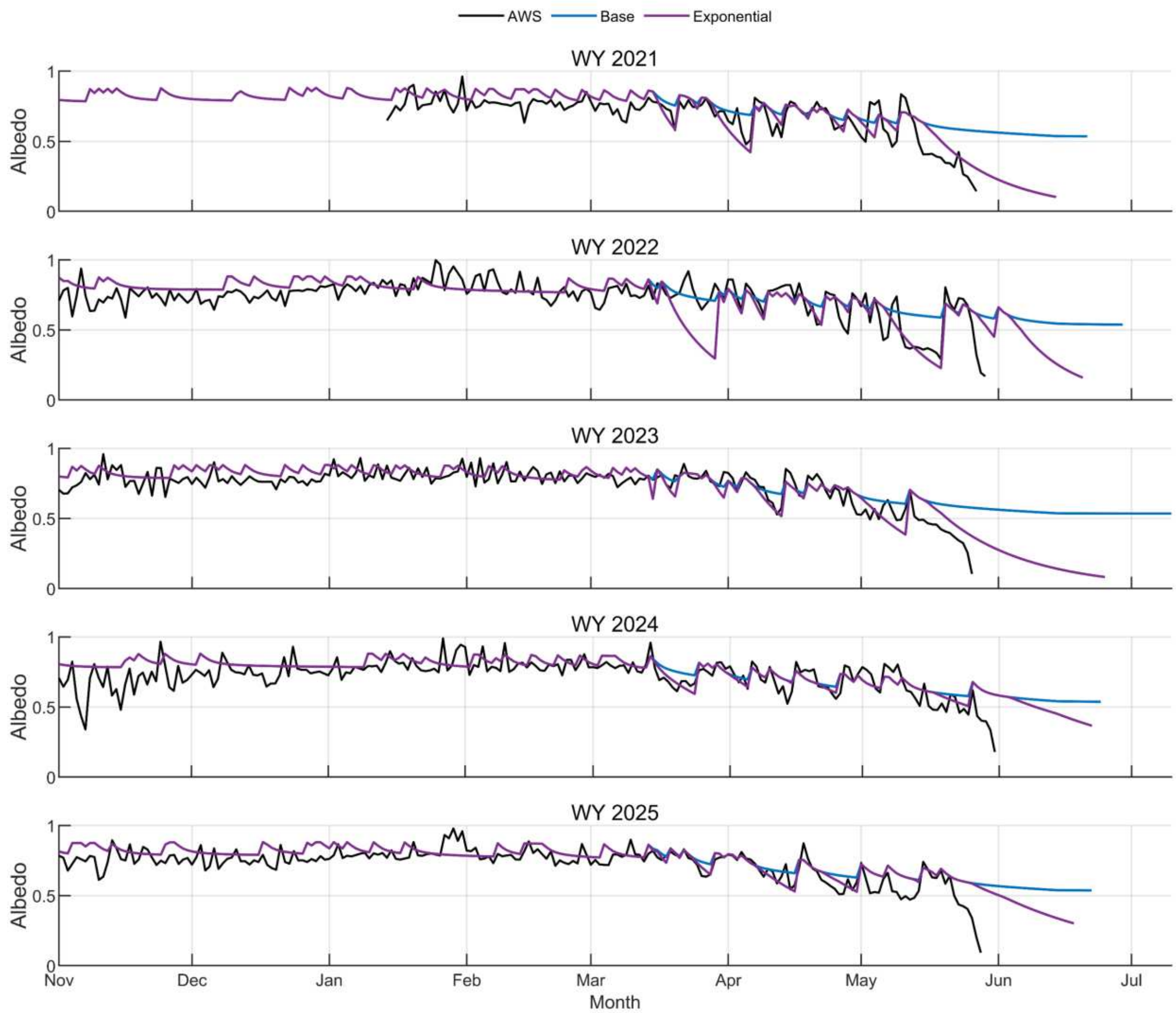

Figure 9. Time series of daily albedo at the Burned Flat AWS site for water years 2021–2025. Observed daily median albedo (black) is compared with the base iSnobal simulation (blue) and the exponential decay albedo simulation (purple). Exponential albedo decay is onset following 15 March.

Modeled albedo under the exponential configuration exhibited greater variability than the base configuration during the ablation period at the Burned Flat AWS station from water years 2021–2025 (Figure 10). While the base run albedo ranged from 0.57 to 0.78, the exponential configuration produced albedo values spanning 0.22 to 0.78. Station observations at Burned Flat AWS exhibited a similar range of variability during the ablation period (0.19– 0.87). Modeled albedo from the combined and LF iSnobal model runs show similar patterns and are included as Supplementary Figure 2.

Across the first three post-fire winters, KS distance between the exponential configuration and observations decreased by 50% to 63% relative to the base configuration (Figure 10). In WY 2024–2025, reductions in KS distance were 25% and 29% respectively. When using the combined exponential decay with LF method, similar reductions in K-S distance relative to observations were identified (50–67% in WY 2021–2023 and 25–29% in WY 2024–2025; Supplementary Figure 3). These results indicated improved agreement between modeled and observed albedo distributions when incorporating exponential decay, particularly in the early post-fire years.

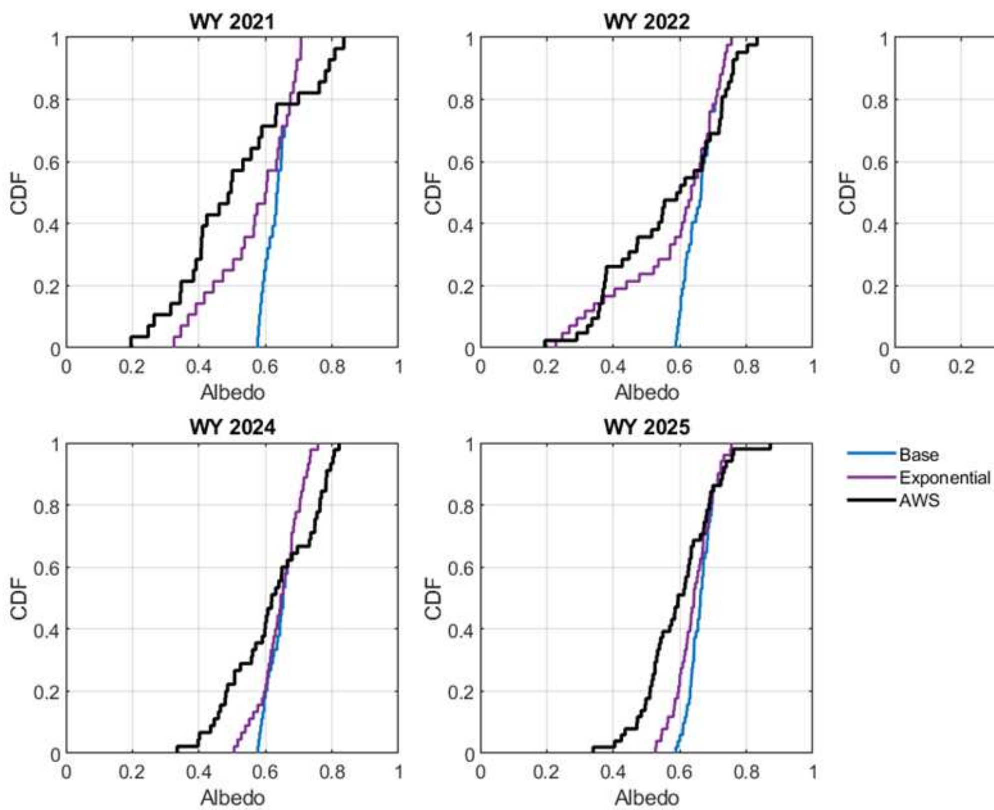

Figure 10. Empirical CDFs of daily snow albedo at the Burned Flat AWS site for water years 2021–2025 during the observed ablation period (AWS peak SWE to snow disappearance).

4.4.3. Melt Rates

Across all water years, melt rates varied within each period and among model configurations (Figure 11). During the peak SWE to SDD period, burned flat AWS melt rates exhibited the greatest variability, with interquartile ranges (IQRs) ranging from 15–28 mm day^{-1}, compared to 12–18 mm day^{-1} for the exponential run and 8–13 mm day^{-1} for the base model. Median AWS melt rates ranged from approximately 9 to 18 mm day^{-1} across the five-year study period, with upper quartiles commonly exceeding 20–25 mm day^{-1}. In comparison, modeled melt rates were typically lower and less variable. The base model consistently exhibited lower melt rates than the AWS in most years, with medians generally between 8 and 12 mm day^{-1}. The exponential run produced higher melt rates than the base model (median 10 –13 mm day^{-1}), which more closely matched AWS medians (1–4 mm day^{-1} improvement) in WY 2022–WY 2024.

During the sustained melt periods, melt rates increased across all datasets and showed greater interannual variability than during the peak SWE to SDD period (Figure 11). AWS melt rates during sustained melt frequently exceeded 30 mm day^{-1} at the upper quartile and reached maxima above 40 mm day^{-1} in WY 2021, WY 2024, and WY 2025. Modeled melt rates remained consistently lower than AWS values in all years. The base model produced the lowest melt medians overall, remaining below 15 mm day^{-1}, while the exponential run showed intermediate melt rates between the AWS observations and base model run, with medians commonly ranging from 10 to 16 mm day^{-1} depending on the year.

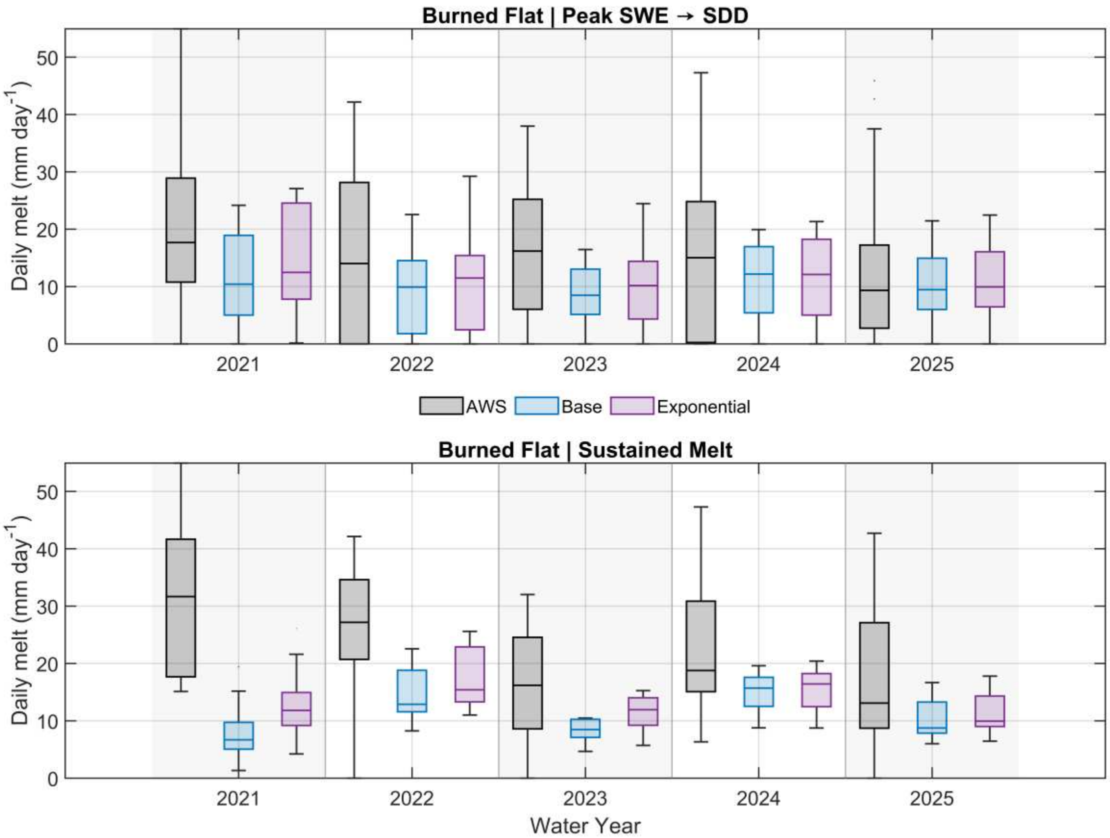

Figure 11. Distribution of daily melt rates at Burned Flat AWS for WY 2021–2025. Melt rates (mm day^{-1}) were computed from daily SWE changes with negative values excluded. Boxplots compare AWS observations with the base and exponential iSnobal runs for the peak SWE to SDD period (top) and a manually defined sustained melt window (bottom). Boxes show the IQR and median; whiskers extend to the maximum and minimum.

4.4.4. Cumulative Net Shortwave Energy

Differences associated with the exponential albedo decay parameterization alone were smaller in magnitude compared to the LF model run configuration (Figure 12). Across burned sites, exponential-base differences in shortwave energy ranged from ~58 to 95 MJ m^{-2} during WY 2021–2023, with the largest increases at Burned North (up to 95 MJ m^{-2}) and Burned Flat (up to 82 MJ m^{-2}; Figure 12; Supplementary Figure 4). Differences were smaller in WY 2024–2025 (16 to 33 MJ m^{-2}) across all burned sites. Similarly, combined–LF differences ranged from

~50 to 125 MJ m⁻², with the largest differences at Burned North in WY 2022 (124 MJ m⁻²), and remained smaller in WY 2024–2025 (25–43 MJ m⁻²).

In contrast, the LF configuration, which accounts for post-fire vegetation changes but retains the base model albedo, consistently absorbed greater cumulative net shortwave energy than the base configuration at burned sites. LF-base differences ranged from 756 to 1,212 MJ m⁻² across burned sites from water years 2021–2025. The differences were largest at Burned South (up to 1,212 MJ m⁻²), followed by Burned Flat (~875–980 MJ m⁻²; Figure 12) and Burned North (~750–825 MJ m⁻²). Across all burned sites and water years, LF–base differences exceeded exponential–base and combined–LF differences.

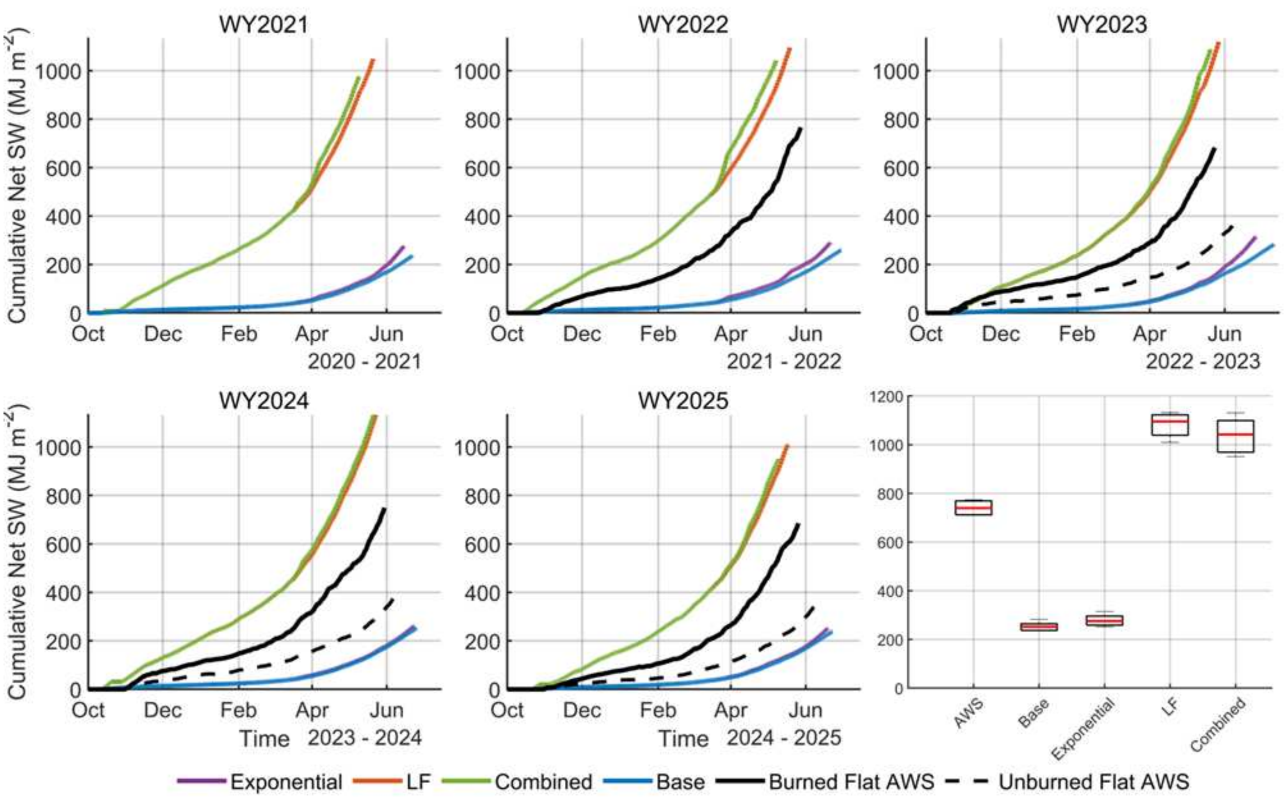

Figure 12. Cumulative net shortwave energy at the Burned Flat AWS site for water years 2021–2025. Panels show cumulative energy from the exponential albedo decay, LF, combined, base model configurations, and AWS observations. Cumulative values are integrated over the snow-covered period for each water year. A box plot shows final cumulative net SW values for each model run/AWS across the study period. AWS data is omitted for WY 2021 due to station installation midway through the winter. Cumulative energy plots for other burned sites are included as Supplementary Figure 4.

5. DISCUSSION

5.1. Post-Fire Albedo Recovery and Decay Dynamics

At the Burned Flat AWS, the station with the longest continuous record, both minimum and median ablation-season albedo were lowest in WY 2021–2022 (minimum 0.19–0.20; median 0.38–0.46) and increased toward their highest values in WY 2024–2025 (minimum 0.33–0.34; median 0.53–0.59; Figure 5). Median albedo increased by ~40% from its lowest value in WY 2022 to WY 2025 (0.38 to 0.53), which likely reflects a reduction in the availability of burned debris and soot with time since fire. While a modest decline in median ablation-season albedo was observed from WY 2024 (0.59) to WY 2025 (0.53), this suggests that albedo recovery is not linear and can be influenced by interannual variability in meteorological conditions.

Decay rates showed a similar pattern, with median rates increasing (less negative) by 38% over the study period (-0.08 day^{-1} in WY 2022 to -0.05 day^{-1} in WY 2025; Figure 6). These results indicated that wildfire impacts on snow albedo persisted for multiple winters but evolved over time. This progression is consistent with field observations, where visibly darker, impurity-rich snow surfaces in May 2021 (first post-fire winter) transitioned to cleaner, higher-albedo conditions by late April 2024 (four years post-fire) at the same site (Burned Flat AWS; Figure 13).

Additionally, photographs from multiple post-fire winters show that trees that were alive pre-fire flake off large sections of charred bark over time and remaining boles have much less soot (Figure 13), especially on west-facing aspects, consistent with scour from the predominant wind direction. In contrast, trees that were already dead pre-fire tend to remain dark-colored and sooty. While qualitative in nature, they clearly illustrate the gradual reduction in available charred material to be deposited on the snow surface through time, likely contributing to the observed recovery in snow albedo.

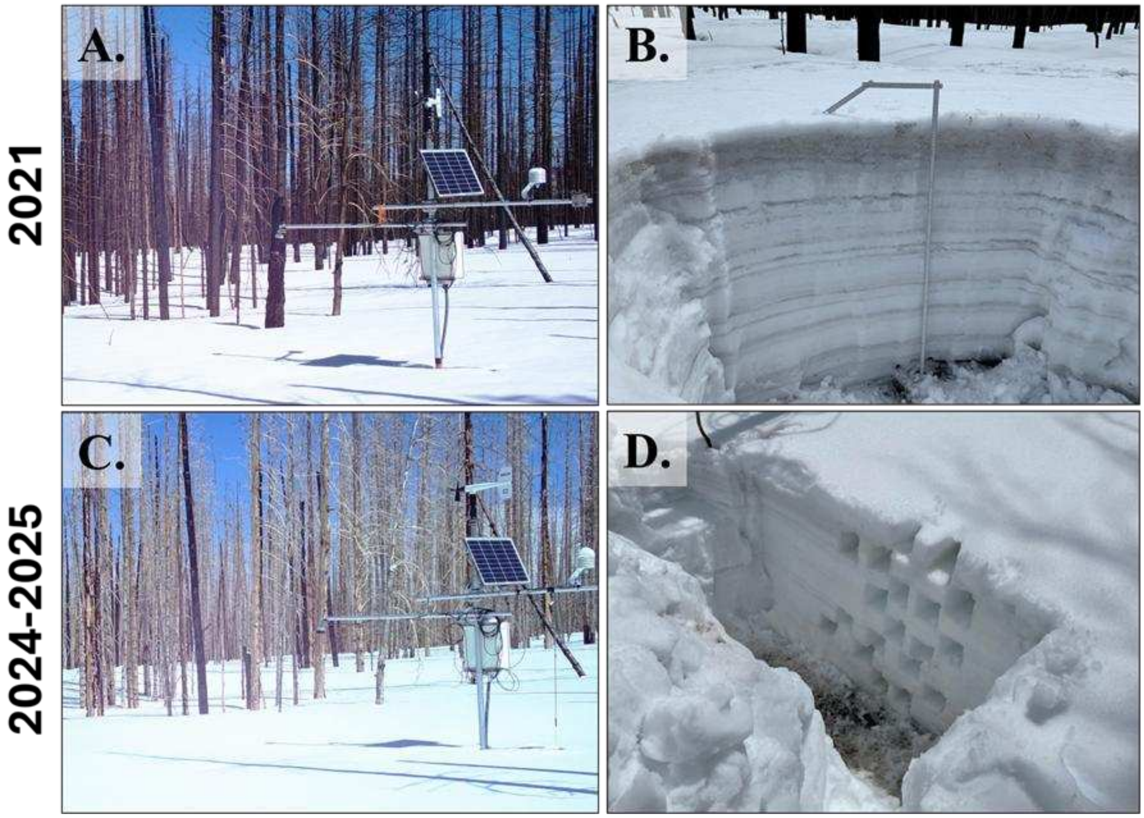

Figure 13. (A) Burned trees at the Burned Flat AWS site during the first post-fire winter, 1 April 2021, (B) Visible soot layers in ablation season snow pit at Burned Flat AWS site, 22 May 2021 (C) Burned trees with charred material flaked off five winters post-fire, 5 April 2025, (D) Ablation season snow pit face showing reduced soot layers at Burned Flat AWS site, 22 April 2024.

Event-scale exponential fits to the observed albedo decay indicated faster and more variable albedo decay at burned sites relative to unburned, particularly in the first two post-fire winters (Figure 6). The fastest albedo decay rates clustered in the melt period (after peak SWE and near snow disappearance), indicating that post-fire albedo conditions strongly influence ablation season snowpack dynamics (Figure 7). At Cameron Pass, frequent late-season snowfall events often reset the snow albedo, which temporarily increases surface reflectivity and buries light-absorbing impurities, leading to reduced net shortwave energy for multiple days and adding mass to the snowpack, thereby extending the snow-covered period. The frequency and timing of these storm-driven resets can regulate the duration of sustained melt conditions by interrupting periods of enhanced radiative forcing and exposure of soot and charred debris at the snow surface (McGrath et al., 2023).

The correlation between decay rate and timing relative to the date of peak SWE was weak when treated as a linear relationship (Figure 7), suggesting that timing alone does not explain variability in decay rate magnitude. However, at burned sites, a greater proportion of decay events occurred after peak SWE, and high-magnitude decay events ($k < -0.10$ day^{-1}) were more frequent, a pattern not observed at unburned sites. Variability in decay rates also increased after peak SWE at burned sites but was relatively consistent at unburned sites (Figure 7). Together, these results suggest that burned site snowpacks exhibit a post-peak SWE regime characterized by more variable and extreme albedo decay compared to unburned conditions.

These patterns indicated that the transition to melt conditions exerts a strong control on decay behavior at burned sites. In the ablation season, higher solar angles and longer days, thinning snowpacks which concentrate soot and debris on the surface, and extended periods without new snow to reset the albedo collectively contribute to accelerated surface darkening and amplified albedo decay. This is further supported by the prior albedo to a storm triggered decay event, where decay events were more negative at burned sites under lower prior albedo conditions (α <0.60; median: −0.06 day^{-1}) compared to higher prior albedo (α >0.60; median: −0.04 day^{-1}), indicating that background surface conditions strongly influenced decay rate behavior (Figure 7). In contrast, weaker relationships at unburned sites (α <0.60; median: −0.032 day^{-1}) compared to higher prior albedo (α >0.60; median: −0.028 day^{-1}) suggests that canopy shading and lower light absorbing impurity inputs limit the variability and magnitude of decay rates. Together, these results showed that decay rates are not simply governed by timing and instead are highly variable with multiple controlling factors, including the post-storm meteorological conditions which are stochastic in nature.

5.2. Implications for Modeling Snow Energy Balance and Melt Timing

In the base iSnobal configuration, modeled broadband snow albedo remained higher and more narrowly distributed than AWS observations, particularly at Burned Flat AWS where modeled albedo did not drop below 0.53 while observed albedo ranged from 0.19 to 0.87 (Figure 9; Figure 10). In the standard configuration, model parameters controlling albedo evolution (e.g., maximum albedo and decay power) are applied uniformly across the entire model domain and cannot be specified separately for burned areas. As a result, the model does not have the ability to represent enhanced albedo decay in post-fire terrain without impacting unburned regions. Along with other factors affecting wildfire-impacted snowpacks, this narrow albedo bias contributed to significantly later modeled SDD, with observed snow disappearance occurring 25–45 days earlier than predicted by the iSnobal base model at Burned Flat AWS (Table 2).

Implementing the field-derived exponential albedo decay parameterization improved agreement between modeled and observed albedo variability and melt dynamics. At Burned Flat AWS, the exponential run shifted SDD earlier by 2–14 days relative to the base configuration, though the model still overpredicted snow disappearance by 18–31 days with similar late melt biases observed at Burned South and Burned North AWS (Table 2). This indicated that while albedo decay is a significant control on melt timing in burned areas, additional processes (e.g., loss of canopy, turbulent fluxes, or forcing data uncertainty) contribute to the remaining late melt out bias. In the base model configuration, the vegetation parameters were based on a pre-fire LANDFIRE dataset and thus did not capture the marked increase in available shortwave radiation in the post-fire forests (Flynn et al., in review). As a result, incoming shortwave radiation at the snow surface remained low relative to observed post-fire conditions, thus limiting the impact of accelerated albedo decay on modeled melt rates. This showed that albedo modifications alone were insufficient to fully capture post-fire changes in snow energy balance when canopy structure is not updated.

The exponential decay method also produced a broader distribution of daily albedo values more closely aligned with AWS observations during the ablation season. KS distance analysis showed a 50–63% reduction in mismatch between modeled and observed albedo CDF distributions in the first three post-fire winters and smaller improvements (25–29%) in WY 2024–2025 (Figure 10). This reduced improvement in later post-fire winters reflects the observed albedo recovery trajectory (Figure 5; Figure 6) as post-fire effects diminish, indicating that time (years) since fire should be accounted for when modeling post-fire snow albedo conditions.

Changes in earlier melt out timing coincided with an increase in absorbed shortwave radiation when using the exponential decay method. The exponential decay method increased cumulative net shortwave absorption relative to the base configuration (55–95 MJ m^{-2} in the first three post-fire winters), and melt rates were correspondingly higher and more closely aligned with AWS observations, particularly during sustained melt periods (Figure 11). Together, these results demonstrated that the post-fire exponential decay method improves modeled snow energy balance and melt timing in a physically consistent manner through increased absorbed shortwave radiation.

5.3. Assessing the Role of Wildfire-Impacted Albedo versus Canopy Loss

Comparisons among the base run, exponential, LF, and combined model runs provide insight into the roles of post-fire canopy loss and snow albedo changes on snowpack dynamics. The LF model runs showed substantially larger increases in cumulative net shortwave energy than the exponential albedo modification alone, with LF-base differences of 756–1,212 MJ m^{-2} across burned sites compared to exponential-base differences of 58–95 MJ m^{-2} during the first three post-fire winters, and near zero differences in years four and five (Figure 12). These findings are consistent with field observations from earlier work at Cameron Pass, which found that the increased incoming shortwave radiation from post-fire canopy loss was six times more impactful in altering net shortwave radiation than declines in snow surface albedo (Reis et al., 2024). Together, these results indicated that forest canopy loss exerts a stronger and more persistent control on post-fire shortwave energy absorption than changes to snow surface albedo alone.

Although forest canopy loss is a stronger control on absorbed shortwave radiation, the exponential decay model runs consistently increased absorbed shortwave radiation and reduced late melt out bias by 2–14 days relative to the base run, particularly during early post-fire winters (Figure 8; Table 2). However, when combined with post-fire canopy loss, the combined LF–exponential model runs often resulted in significantly earlier snow disappearance than observed and standard LF model runs (Table 2), in some cases up to 22 days too early at Burned Flat AWS in WY 2022. This suggests that applying both effects simultaneously may overamplify energy inputs during the ablation period, indicating that the loss of canopy and reduced snow albedo require more tightly constrained parameterizations when used together in post-fire snowpack energy balance modeling.

Additionally, these results indicated that post-fire albedo recovery and vegetation recovery occur on different time scales. Snow albedo may recover relatively quickly (≤5 years; Figure 5) as the available supply of charred material in burned landscapes declines through time (Figure 13), consistent with observations that post-fire forests act as a persistent but diminishing source of black carbon to the snowpack over decadal timescales (Uecker et al., 2020). In contrast, recovery of forest canopy structure occurs over much longer timescales and may never fully recover following high-severity fires (Coop et al., 2022; Stevens-Rumann and Morgan, 2019).

5.4. Modeling Assumptions and Transferability

As the primary objective of this study was to improve albedo evolution in burned areas, exponential albedo decay parameterization was only applied to burned areas within the iSnobal model domain. However, our field observations showed substantial spatiotemporal variability in the accumulation of forest litter in the unburned forests, highlighting an important area of future research (Supplementary Figure 5).

The exponential decay formulation in this study applied a single median decay rate uniformly across burned areas. In reality, albedo decay rates likely vary across burn severities, vegetation structures, and local topography. The use of a binary burned/unburned application of exponential albedo decay restricts spatial heterogeneity in post-fire albedo processes and should be addressed in future work. Additionally, the use of a single median albedo decay rate limits representation of temporal variability in decay behavior, as results show decay rates are not static through time (Figure 7). Incorporating albedo decay parameterizations that vary with burn severity would provide a more physically realistic method for representing heterogeneous post-fire landscapes and help resolve differences observed in previous studies (e.g., Gleason and Nolin, 2016; Surunis and Gleason, 2024).

Improvements in modeled albedo representation were only possible because field observations were available to retrospectively constrain albedo decay rates. In basins without this in-situ record, post-fire decay rates could be implemented by i) applying published values from similar burned environments, ii) developing relationships based on burn severity, or iii) implementing remotely sensed albedo products (e.g., Meyer et al., 2024).

While results showed substantial recovery over the study period, this study is limited to five post-fire winters (2021–2025) at a single site within a continental snow climate, which constrains inferences about longer term albedo recovery processes and transferability to other snow climate regimes. Maritime snow climates, such as the Cascades and Sierra Nevada, are more strongly dominated by cloud cover and winter atmospheric rivers that drive rapid accumulation, while continental regions experience lower-intensity frontal storms and more frequent but less intense spring precipitation, leading to longer accumulation seasons and later onset of melt (Serreze et al., 1999; Trujillo and Molotch, 2014). These differences may limit the duration of exposed snow aging surfaces compared to a continental snow climate like Cameron Pass.

Despite these differences, observations from burned forests in Oregon's Cascades show that rapid post-fire albedo decay events still occur (Gleason and Nolin, 2016), and recent work in the Sierra Nevada indicates that extended dry periods can enhance post-fire melt in maritime snow climate regimes (Hatchett et al., 2023). This suggests that while the magnitude and persistence of post-fire albedo effects vary by snow climate, the underlying processes linking snow surface darkening to increased melt are consistent across regions.

Additionally, iSnobal model forcing data introduces uncertainty in these results. Atmospheric forcing data for all model runs was derived from the HRRR dataset at 3 km spatial resolution, which may not fully capture meteorological variability in mountainous terrain. Errors in precipitation quantity and timing affect the timing of albedo reset and persistence of albedo decay, which are critical in all modeling configurations (Figure 9; example 23 March 2022 storm event). Misrepresentation of snowfall events therefore propagates into subsequent albedo evolution and absorbed shortwave radiation, which affects melt timing and magnitude. Additional uncertainties in shortwave radiation inputs, cloud cover, and temperature at this resolution can affect modeled snowpack dynamics, which are consistent with other studies on mountain snow modeling (e.g., Havens et al., 2020; Meyer et al., 2023).

6. FUTURE WORK

Building on the results of this thesis and previous studies, future work should focus on improving representation of spatial and temporal variability in post-fire snow albedo processes. In this study, a single median exponential decay rate was applied uniformly across burned areas in iSnobal due to a limited number of observation sites in a single watershed. However, results indicate that albedo decay rates vary with snowpack conditions, timing relative to snowpack conditions (i.e., before/after peak SWE), and background albedo prior to a snowfall event (Figure 7). While additional observations could help constrain these dynamics, albedo decay is inherently variable and strongly influenced by site-specific conditions. As a result, representing albedo decay with a single uniform decay rate may not capture the natural variability of albedo evolution across time and space. The single uniform decay rate is an easier modeling implementation, but future model approaches may benefit from incorporating snow state-dependent or conditionally varying parameterizations that better reflect the range of observed behavior.

Future work should therefore focus not only on increasing the number of observation sites, but also on better characterizing the controls on albedo decay behavior. Albedo decay rates are influenced by snowpack conditions such as temperature, presence of liquid water, periods of sustained melt, and storm characteristics, which govern snow grain growth, impurity exposure, and the rate at which the snow surface darkens. In addition, site-dependent factors such as tree density, burn severity, pre-fire tree conditions (i.e., live vs. dead), the persistence and redistribution of soot on tree boles, and wind exposure likely play important roles in post-fire albedo evolution. Detailed field observations targeting these processes, particularly in the immediate post-fire winter, would improve understanding of early post-fire conditions when albedo impacts are most pronounced. Expanding observation networks immediately following disturbance and incorporating these site-specific controls into model parametrizations may provide a pathway towards a more physically realistic representation of post-fire albedo decay dynamics.

Representation of spatial heterogeneity is also limited by the binary burn/unburned classification applied in the iSnobal model domain in this study. This approach was chosen due to a limited number of observation sites placed in high burn severities, and for simplicity in implementing spatially varying albedo decay between burned and unburned regions. This approach, however, does not capture variability in burn severity or vegetation structure, both of which influence shortwave radiation absorbed by the snowpack through differences in canopy cover and the availability of light-absorbing material on the snow surface. Existing datasets such as MTBS and LANDFIRE provide a pathway for implementing burn severity dependent parameterization and could be combined with remotely sensed albedo products (i.e., MODIS and VIIRS) to constrain spatial patterns beyond point-scale observations. Recent work has shown that improved representation of net solar radiation and albedo using incoming solar radiation output from HRRR and remotely sensed albedo from MODIS improves iSnobal model simulations relative to in situ observations (Meyer et al., 2024). Future efforts could combine the spatial coverage of remotely sensed albedo products with high-resolution point-scale observations to further constrain natural variability in albedo decay across burn severities for implementation in snow energy balance models.

Additional considerations include uncertainties in meteorological forcing, which remains a primary limitation for modeling snowpack evolution in complex mountainous terrain. In this study, HRRR forcing data at 3 km resolution was used in iSnobal combined with SMRF terrain adjustments, which does not fully represent small scale variability in precipitation, radiation, and temperature. These uncertainties directly affect albedo reset events, energy input, and melt timing. Future work should evaluate performance of higher resolution forcing datasets or downscaling approaches in iSnobal simulations. While this study focused on improved model parameterizations in burned areas, improvements in forcing data are likely to be just as important for reducing uncertainty in simulated snow energy balance.

Further work could follow the approach outlined in this study in another watershed and snow climate regime for assessment of transferability in model improvements. While this study was performed in a continental snow climate, where relatively shallow snowpacks and high springtime solar radiation may amplify the effects of albedo decay, these environments are also subject to frequent late-spring snowfall events that reset surface albedo and prolong snow persistence (McGrath et al., 2023). This interplay between rapid albedo decay conditions and frequent reset is likely and important control on melt dynamics in continental systems. Expanding observations across maritime and intermountain regimes would help determine the extent to which these processes and associated parameterizations apply across regions with differing storm frequency and energy balance conditions. Conducting modeling experiments that modify or remove albedo reset mechanisms in the ablation season (e.g., after peak SWE) could help isolate the relative importance of albedo decay versus the frequency of snowfall driven albedo resets in controlling snow disappearance timing.

While this study analyses five years of post-fire albedo behavior, longer term observations are needed to constrain patterns in post-fire recovery trajectories. The results of this study likely reflect interannual variability in snowpack behavior due to differences in meteorological conditions, and additional years of observations could reveal clearer patterns in variability attributed to post-fire impacts. Cameron Pass offers a unique study area for capturing the long-term recovery patterns in a high elevation, snow-dominated watershed and should continue to be studied beyond the five–years of observations presented here.

Finally, future work should focus on the relationship between post-fire impacts on snow energy balance and the broader watershed-scale hydrologic response through time. While this study focuses on improvements in post-fire snowpack evolution, including snow disappearance timing and melt dynamics, these changes ultimately influence runoff timing, peak streamflow, and downstream water availability. Combining snow energy balance models with hydrologic models would provide better evaluation of how post-fire snow dynamics are felt throughout the hydrologic system, which is critical for supporting water resource management in snow-dominated watersheds.

7. CONCLUSIONS

This study investigated five years of post-fire changes in snow albedo following the 2020 Cameron Peak fire in north-central Colorado and implemented field informed parameters to improve performance of a snow energy balance model in burned areas. At the Burned Flat AWS site, minimum and median ablation season albedo increased from 0.19–0.20 and 0.38–0.46 in the first two post-fire winters to 0.34 and 0.53 by 2025, indicating gradual recovery over five post-fire winters. Event-scale analysis showed persistently faster and more variable albedo decay at burned sites compared to unburned, with the largest-magnitude decay events occurring after peak SWE and near SDD when the pre-storm albedo was low. Together, these results demonstrated that both ablation season albedo and albedo decay are important controls on post-fire snowpack dynamics for multiple years following a wildfire.

Incorporating field-derived exponential albedo decay rates into the iSnobal model improved agreement of modeled snow surface albedo with observations in burned terrain. Relative to the base configuration, the exponential formulation produced greater variability in modeled albedo, improving agreement with observations, and shifted modeled snow disappearance up to 16 days earlier days at burned sites. These improvements coincided with an increase in cumulative net shortwave absorption (55–95 MJ m^{-2} increase in first three winters), and melt rates more closely aligned with observations, indicating that the albedo modifications improved modeled snow energy balance in a physically meaningful way. Additional model experiments incorporating post-fire vegetation changes showed that canopy loss exerted a stronger and more persistent influence on absorbed shortwave radiation than albedo changes alone, highlighting the importance of representing both vegetation and snow albedo changes in post-fire modeling frameworks.

These findings demonstrated that default albedo parameterizations in iSnobal underestimate the magnitude and timing of snowmelt in burned areas, especially during the first post-fire winters. Incorporating field-derived parameters for post-fire snow albedo decay improved modeled simulations of snow energy balance and melt timing to better support water supply forecasting in wildfire impacted headwaters regions. As wildfire activity continues to increase across snow-dominated landscapes in the Western United States, improved representation of their impacts on snow processes in snow energy balance models is increasingly important when accounting for shifts in snowmelt timing and downstream water availability.

REFERENCES

Abatzoglou, J. T., & Williams, A. P. (2016). Impact of anthropogenic climate change on wildfire across western U.S. forests. *Proceedings of the National Academy of Sciences*, 113(42), 11770–11775. https://doi.org/10.1073/pnas.1607171113

Anderson, E. A. (1976). *A point energy and mass balance model of a snow cover*. NOAA Technical Report NWS 19.

Barnett, T. P., Adam, J. C., & Lettenmaier, D. P. (2005). Potential impacts of a warming climate on water availability in snow-dominated regions. *Nature*, 438(7066), 303–309. https://doi.org/10.1038/nature04141

Benjamin, S. G., Weygandt, S. S., Brown, J. M., Hu, M., Alexander, C. R., Smirnova, T. G., et al. (2016). A North American hourly assimilation and model forecast cycle: The rapid refresh. *Monthly Weather Review*, 144, 1669–1694. https://doi.org/10.1175/MWR-D-15-0242.1

Bonnell, R., Tarricone, J., Marshall, H.-P., Deeb, E., & Vuyovich, C. (2025). Satellite radar advances could transform global snow monitoring. *Eos*, 106. https://doi.org/10.1029/2025EO250476

Burles, K., & Boon, S. (2011). Snowmelt energy balance in a burned forest plot, Crowsnest Pass, Alberta, Canada. *Hydrological Processes*, 25(19), 3012–3029. https://doi.org/10.1002/hyp.8067

Clark, M. P., Hendrikx, J., Slater, A. G., Kavetski, D., Anderson, B., Cullen, N. J., et al. (2011). Representing spatial variability of snow water equivalent in hydrologic and land-surface models: A review. *Water Resources Research*, *47*(7), 2011WR010745. https://doi.org/10.1029/2011WR010745

Clow, D. W. (2010). Changes in the timing of snowmelt and streamflow in Colorado: A response to recent warming. *Journal of Climate*, 23(9), 2293–2306. https://doi.org/10.1175/2009JCLI2951.1

Coop, J. D., Parks, S. A., Stevens-Rumann, C. S., Crausbay, S. M., Higuera, P. E., Hurteau, M. D., et al. (2022). Wildfire-driven forest conversion in western North American landscapes. *BioScience*, 72(7), 622–643. https://doi.org/10.1093/biosci/biac031

Dyunin, A. K., & Kotlyakov, V. M. (1980). Redistribution of snow in the mountains under the effect of heavy snow-storms. *Cold Regions Science and Technology*, 3(4), 287–294. https://doi.org/10.1016/0165-232X(80)90035-X

Eidenshink, J., Schwind, B., Brewer, K., Zhu, Z.-L., Quayle, B., & Howard, S. (2007). A Project for Monitoring Trends in Burn Severity. *Fire Ecology*, *3*(1), 3–21. https://doi.org/10.4996/fireecology.0301003

Essery, R., Morin, S., Lejeune, Y., & B Ménard, C. (2013). A comparison of 1701 snow models using observations from an alpine site. *Advances in Water Resources*, *55*, 131–148. https://doi.org/10.1016/j.advwatres.2012.07.013

Flynn, H., McGrath, D., Meyer, J., Caldwell, N. G., Stevens-Rumann, C., Kampf, S. K., Fassnacht, S. R., Hedrick, A. R., Elder, K., & Reis, W. (2026). *Evaluating the influence of vegetation parameters in a snow energy and mass balance model in wildfire-impacted landscapes*. Unpublished manuscript.

Gagliano, E., Shean, D., Henderson, S., & Vanderwilt, S. (2023). Capturing the Onset of Mountain Snowmelt Runoff Using Satellite Synthetic Aperture Radar. *Geophysical Research Letters*, *50*. https://doi.org/10.1029/2023GL105303

Garen, D. C., & Marks, D. (2005). Spatially distributed energy balance snowmelt modeling in a mountainous watershed: Model development and application. *Water Resources Research*, 41(11), W10414.

Gayler, J. M., & Skiles, S. M. (2024). Response of land surface albedo to fire disturbance in the Sierra Nevada seasonal snow zone over the MODIS record. *Earth's Future*, 12(6), e2023EF004172. https://doi.org/10.1029/2023EF004172

Gersh, M., Gleason, K. E., & Surunis, A. (2022). Forest fire effects on landscape snow albedo recovery and decay. *Remote Sensing*, 14(16), 4079. https://doi.org/10.3390/rs14164079

Gleason, K. E., & Nolin, A. W. (2016). Charred forests accelerate snow albedo decay: Parameterizing the post-fire radiative forcing on snow for three years following fire. *Hydrological Processes*, 30(21), 3855–3870. https://doi.org/10.1002/hyp.10897

Hale, K. E., Jennings, K. S., Musselman, K. N., Livneh, B., & Molotch, N. P. (2023). Recent decreases in snow water storage in western North America. *Communications Earth & Environment*, 4, 1–11. https://doi.org/10.1038/s43247-023-00751-3

Hall, D. K., & Riggs, G. A. (2007). Accuracy assessment of the MODIS snow products. *Hydrological Processes*, 21(12), 1534–1547. https://doi.org/10.1002/hyp.6715

Hatchett, B. J., Koshkin, A. L., Guirguis, K., Rittger, K., Nolin, A. W., Heggli, A., et al. (2023). Midwinter dry spells amplify post-fire snowpack decline. *Geophysical Research Letters*, 50(3), e2022GL101235. https://doi.org/10.1029/2022GL101235

Havens, S., Marks, D., Sandusky, M., Hedrick, A., Johnson, M., Robertson, M., & Trujillo, E. (2020). Automated water supply model (AWSM): Streamlining and standardizing application of a physically based snow model for water resources and reproducible science. *Computers & Geosciences*, 144, 104571. https://doi.org/10.1016/j.cageo.2020.104571

Havens, S., Marks, D., Kormos, P., Hedrick, A., Trujillo, E., Johnson, M., et al. (2022). Spatial Modeling for Resources Framework (SMRF). Zenodo. https://doi.org/10.5281/zenodo.6543935

Hedstrom, N. R., & Pomeroy, J. W. (1998). Measurements and modelling of snow interception in the boreal forest. *Hydrological Processes*, *12*(10–11), 1611–1625. https://doi.org/10.1002/(SICI)1099-1085(199808/09)12:10/11<1611::AID-HYP684>3.0.CO;2-4

Iglesias, V., Balch, J. K., & Travis, W. R. (2022). U.S. fires became larger, more frequent, and more widespread in the 2000s. *Science Advances*, 8(11), eabc0020. https://doi.org/10.1126/sciadv.abc0020

Joachim Meyer, Michelle Hu, Joe Ammatelli, prkormos, Scott Havens, Micah Sandusky, & Micah Johnson. (2026, May 21). iSnobal/awsm: v20260520 (Version 20260520). Zenodo. https://doi.org/10.5281/ZENODO.20328895

Kampf, S. K., McGrath, D., Sears, M. G., Fassnacht, S. R., Kiewiet, L., & Hammond, J. C. (2022). Increasing wildfire impacts on snowpack in the western U.S. *Proceedings of the National Academy of Sciences*, 119(39), e2200333119. https://doi.org/10.1073/pnas.2200333119

Koshkin, A. L., Hatchett, B. J., & Nolin, A. W. (2022). Wildfire impacts on western United States snowpacks. *Frontiers in Water*, *4*. https://doi.org/10.3389/frwa.2022.971271

Key, J. R., Mahoney, R., Liu, Y., Romanov, P., Tschudi, M., Appel, I., et al. (2013). Snow and ice products from Suomi NPP VIIRS. *Journal of Geophysical Research: Atmospheres*, *118*(23), 12,816-12,830. https://doi.org/10.1002/2013JD020459

Li, D., Wrzesien, M. L., Durand, M., Adam, J., & Lettenmaier, D. P. (2017). How much runoff originates as snow in the western United States, and how will that change in the future? *Geophysical Research Letters*, 44(12), 6163–6172. https://doi.org/10.1002/2017GL073551

Link, T., & Marks, D. (1999). Distributed simulation of snowcover mass- and energy-balance in the boreal forest. *Hydrological Processes*, *13*(14–15), 2439–2452. https://doi.org/10.1002/(SICI)1099-1085(199910)13:14/15<2439::AID-HYP866>3.0.CO;2-1

Liston, G. E., & Sturm, M. (1998). A snow-transport model for complex terrain. *Journal of Glaciology*, *44*(148), 498–516. https://doi.org/10.3189/S0022143000002021

Lyons, E., Jin, Y., & Randerson, J. (2008). Changes in surface albedo after fire in boreal forest ecosystems of interior Alaska assessed using MODIS satellite observations. *Journal of Geophysical Research*, 113, G02012. https://doi.org/10.1029/2007JG000606

Marks, D., & Dozier, J. (1992). Climate and energy exchange at the snow surface in the alpine region of the Sierra Nevada: 2. Snow cover energy balance. *Water Resources Research*, 28(11), 3043–3054. https://doi.org/10.1029/92WR01483

Marks, D., Domingo, J., Susong, D., Link, T., & Garen, D. (1999). A spatially distributed energy balance snowmelt model for application in mountain basins. *Hydrological Processes*, 13(12–13), 1935–1959. https://doi.org/10.1002/(SICI)1099-1085(199909)13:12/13<1935::AID-HYP868>3.0.CO;2-C

Marks, D., Winstral, A., Reba, M., Pomeroy, J., & Kumar, M. (2013). An evaluation of methods for determining snowfall catch correction factors at instrumented sites. *Journal of Hydrometeorology*, 14, 1275–1287

Marshall, S. E., & Warren, S. G. (1987). Parameterization of snow albedo for climate models. In *Large scale effects of seasonal snow cover* (IAHS Publication No. 166)

McGrath, D., Zeller, L., Bonnell, R., Reis, W., Kampf, S., Williams, K., et al. (2023). Declines in peak snow water equivalent and elevated snowmelt rates following the 2020 Cameron Peak wildfire in northern Colorado. *Geophysical Research Letters*, 50(6), e2022GL101294. https://doi.org/10.1029/2022GL101294

Meyer, J., Horel, J., Kormos, P., Hedrick, A., Trujillo, E., & Skiles, S. M. (2023). Operational water forecast ability of the HRRR–iSnobal combination: An evaluation to adapt into production environments. *Geoscientific Model Development*, 16(1), 233–250. https://doi.org/10.5194/gmd-16-233-2023

Meyer, J., Hedrick, A., & McKenzie Skiles, S. (2024). A new approach to net solar radiation in a spatially distributed snow energy balance model to improve snowmelt timing. *Journal of Hydrology*, *638*, 131490. https://doi.org/10.1016/j.jhydrol.2024.131490

Mote, P. W., Li, S., Lettenmaier, D. P., Xiao, M., & Engel, R. (2018). Dramatic declines in snowpack in the western U.S. *npj Climate and Atmospheric Science*, 1, 1–6. https://doi.org/10.1038/s41612-018-0012-1

Mote, P. W., A. F. Hamlet, M. P. Clark, and D. P. Lettenmaier (2005), Declining mountain snowpack in western North America, *Bull. Am. Meteorol. Soc.*, **86**(1), 39–49. https://doi.org/10.1175/BAMS-86-1-39

Nagler, T., Rott, H., Ripper, E., Bippus, G., & Hetzenecker, M. (2016). Advancements for Snowmelt Monitoring by Means of Sentinel-1 SAR. *Remote Sensing*, *8*(4), 348. https://doi.org/10.3390/rs8040348

Painter, T. H., Barrett, A. P., Landry, C. C., Neff, J. C., Cassidy, M. P., Lawrence, C. R., et al. (2007). Impact of disturbed desert soils on duration of mountain snow cover. *Geophysical Research Letters*, 34(12), L12502. https://doi.org/10.1029/2007GL030284

Painter, T. H., Skiles, S. M., Deems, J. S., Bryant, A. C., & Landry, C. C. (2012). Dust radiative forcing in snow of the Upper Colorado River Basin: 1. A 6 year record of energy balance, radiation, and dust concentrations. *Water Resources Research*, 48(7), W07521. https://doi.org/10.1029/2012WR011985

Painter, T. H., Berisford, D. F., Boardman, J. W., Bormann, K. J., Deems, J. S., Gehrke, F., et al. (2016). The Airborne Snow Observatory: Fusion of scanning lidar, imaging spectrometer, and physically-based modeling for mapping snow water equivalent and snow albedo. *Remote Sensing of Environment*, *184*, 139–152. https://doi.org/10.1016/j.rse.2016.06.018

Palomaki, R. T., Rittger, K., Lenard, S. J. P., Bair, E., Dozier, J., Skiles, S. M., & Painter, T. H. (2025). Assessment of methods for mapping snow albedo from MODIS. *Remote Sensing of Environment*, *326*, 114742. https://doi.org/10.1016/j.rse.2025.114742

Parks, S. A., & Abatzoglou, J. T. (2020). Warmer and drier fire seasons contribute to increases in area burned at high severity in western U.S. forests from 1985 to 2017. *Geophysical Research Letters*, 47(22), e2020GL089858. https://doi.org/10.1029/2020GL089858

Pomeroy, J. W., Parviainen, J., Hedstrom, N., & Gray, D. M. (1998). Coupled modelling of forest snow interception and sublimation. *Hydrological Processes*, *12*(15), 2317–2337. https://doi.org/10.1002/(SICI)1099-1085(199812)12:15<2317::AID-HYP799>3.0.CO;2-X

Pomeroy, J., & Gray, D. (1995). Snowcover: Accumulation, Relocation, and Management. *Bulletin of the International Society of Soil Science (Vol. 7)*.

Reis, W., McGrath, D., Elder, K., Kampf, S., & Rey, D. (2024). Quantifying aspect-dependent snowpack response to high-elevation wildfire in the southern Rocky Mountains. *Water Resources Research*. https://doi.org/10.1029/2023WR036539

Rittger, K., Lenard, S. J., Palomaki, R. T., Brodzik, M. J., Stillinger, T., Bair, E. H., et al. (2024). Historical MODIS/Terra L3 global daily 500 m SIN grid snow cover, snow albedo, and snow physical properties (STC_MODSCGDRF_HIST, Version 1) [Data set]. National Snow and Ice Data Center, Boulder, CO. https://doi.org/10.7265/f6j3-f387

Rollins, M. G. (2009). LANDFIRE: A nationally consistent vegetation, wildland fire, and fuel assessment. *International Journal of Wildland Fire*, 18(3), 235–249. https://doi.org/10.1071/WF08088

Schaaf, C. B., Gao, F., Strahler, A. H., Lucht, W., Li, X., Tsang, T., et al. (2002). First operational BRDF, albedo nadir reflectance products from MODIS. *Remote Sensing of Environment*, 83(1), 135–148. https://doi.org/10.1016/S0034-4257(02)00091-3

Schwartz, A. J., McGowan, H., & Callow, N. (2020). Impact of fire on montane snowpack energy balance in snow gum forest stands. *Agricultural and Forest Meteorology*, 294, 108164. https://doi.org/10.1016/j.agrformet.2020.108164

Serreze, M. C., Clark, M. P., Armstrong, R. L., McGinnis, D. A., & Pulwarty, R. S. (1999). Characteristics of the western United States snowpack from snowpack telemetry (SNOTEL) data. *Water Resources Research*, 35(7), 2145–2160. https://doi.org/10.1029/1999WR900090

Sexstone, G. A., Clow, D. W., Fassnacht, S. R., Liston, G. E., Hiemstra, C. A., Knowles, J. F., & Penn, C. A. (2018). Snow sublimation in mountain environments and its sensitivity to forest disturbance and climate warming. *Water Resources Research*, 54, 1191–1211. https://doi.org/10.1002/2017WR021172

Skiles, S. M., Flanner, M., Cook, J. M., Dumont, M., & Painter, T. H. (2018). Radiative forcing by light-absorbing particles in snow. *Nature Climate Change*, 8(11), 964–971. https://doi.org/10.1038/s41558-018-0296-5

Stevens-Rumann, C. S., & Morgan, P. (2019). Tree regeneration following wildfires in the western U.S.: A review. *Fire Ecology*, 15(1), 1–17. https://doi.org/10.1186/s42408-019-0032-1

Surunis, A., & Gleason, K. E. (2024). Modelling postfire recovery of snow albedo and forest structure to understand drivers of decades of reduced snow water storage and advanced snowmelt timing. *Hydrological Processes*, *38*(7), e15246. https://doi.org/10.1002/hyp.15246

Trujillo, E., & Molotch, N. P. (2014). Snowpack regimes of the western United States. *Water Resources Research*, 50(7), 5611–5623. https://doi.org/10.1002/2013WR014753

Uecker, T. M., Kaspari, S. D., Musselman, K. N., & Skiles, S. M. (2020). The post-wildfire impact of burn severity and age on black carbon snow deposition and implications for snow water resources, Cascade Range, Washington. *Journal of Hydrometeorology*, 21(8), 1777–1792. https://doi.org/10.1175/JHM-D-20-0010.1

Ulaby, F.T., Moore, R.K. and Fung, A.K. (1986) Microwave Remote Sensing Active and Passive. Vol. 2. Radar Remote Sensing and Surface Scattering and Emission Theory. Ch. 12, Artech House Publishers, Norwood, 962-966.

U.S. Geological Survey (USGS) and U.S. Forest Service (USFS) (n.d.). *BAER soil burn severity data (MTBS)*. https://www.mtbs.gov/baer (accessed 2026).

Westerling, A. L., Hidalgo, H. G., Cayan, D. R., & Swetnam, T. W. (2006). Warming and earlier spring increase western U.S. forest wildfire activity. *Science*, 313(5789), 940–943. https://doi.org/10.1126/science.1128834

Wang, X., Schaaf, C. B., Sun, Q., Shuai, Y., & Román, M. O. (2020). Capturing rapid land surface dynamics with MODIS BRDF/albedo products. *Remote Sensing of Environment*, 252, 112188. https://doi.org/10.1016/j.rse.2020.112188

SUPPLEMENTARY FIGURES

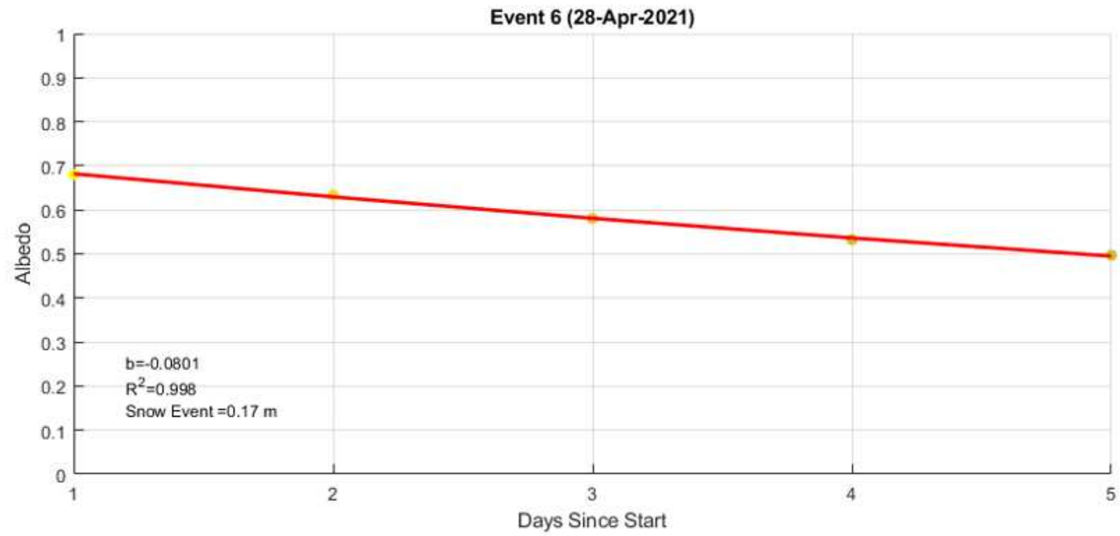

Supplementary Figure 1. Example of exponential regression fit to albedo decay event at Burned Flat AWS station on 28 April 2021.

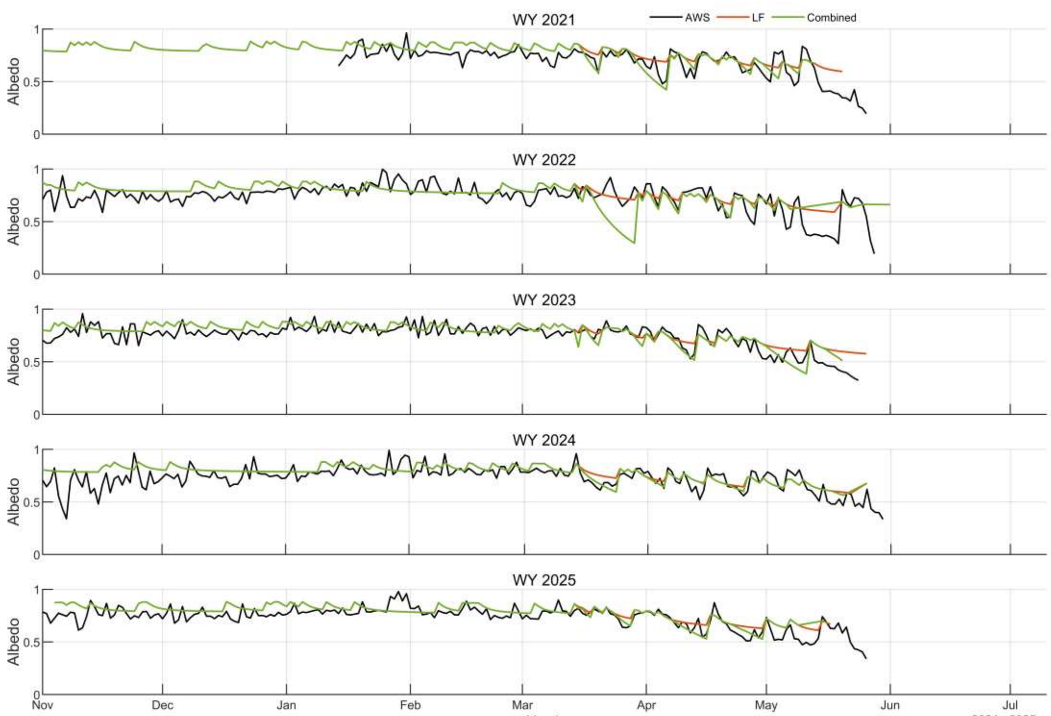

Supplementary Figure 2. Time series of daily albedo at the Burned Flat AWS site for water years 2021–2025. Observed daily median albedo (black) is compared with the LF iSnobal simulation (orange) and the LF combined exponential decay albedo simulation (green). Exponential albedo decay is onset following 15 March.

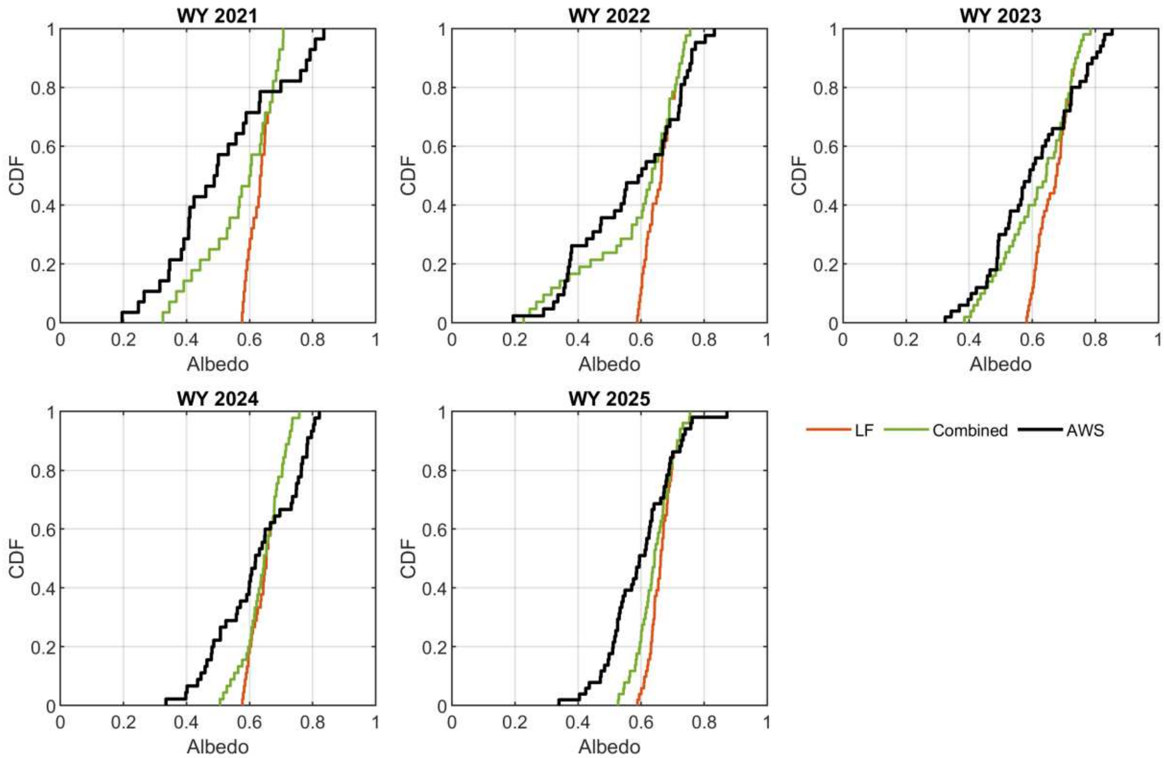

Supplementary Figure 3. Empirical CDFs of daily snow albedo at the Burned Flat AWS site for water years 2021–2025 during the observed ablation period (AWS peak SWE to snow disappearance). Observed albedo (black) is compared with the LF iSnobal simulation (orange) and the combined LF and exponential decay albedo simulation (green).

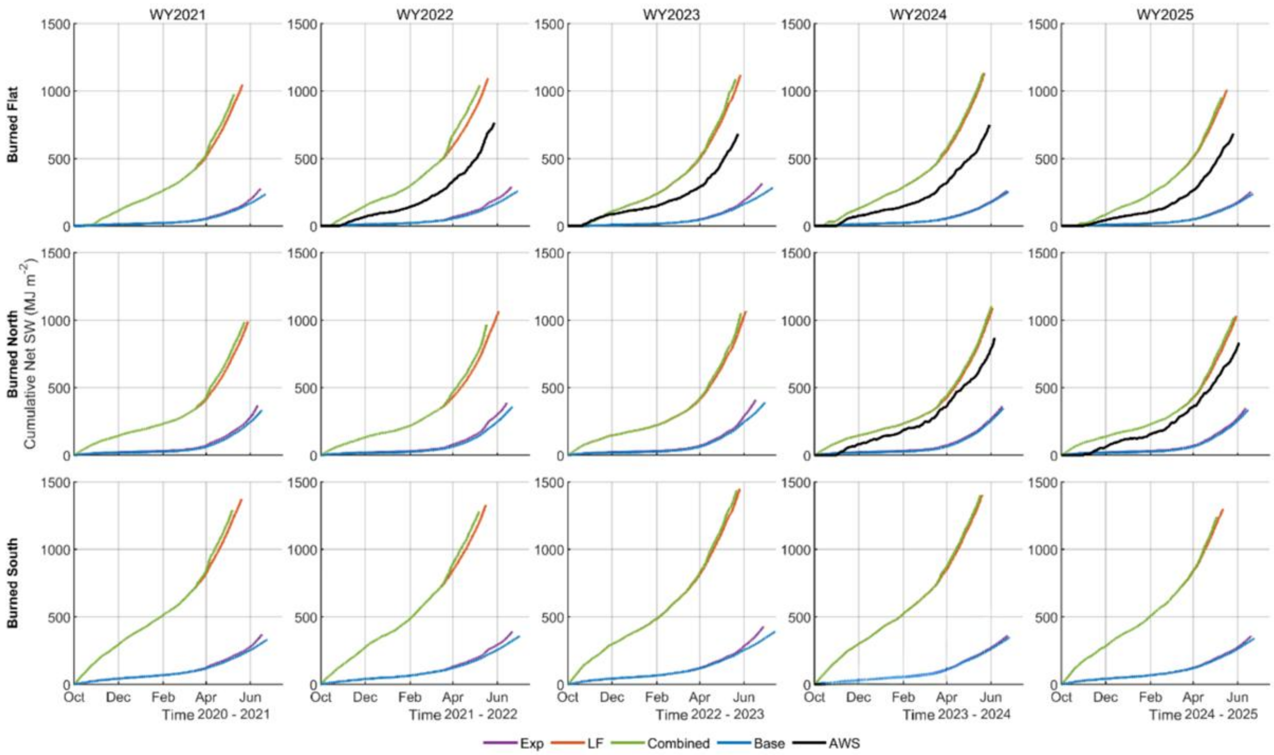

Supplementary Figure 4. Cumulative net shortwave energy at the Burned AWS sites for water years 2021–2025. Panels show cumulative energy from the exponential albedo decay, LF, combined, base model configurations, and AWS observations when available. Cumulative values are integrated over the snow-covered period for each water year.

Supplementary Figure 5. Forest litter deposited on snowpack at the Unburned Flat AWS station in May 2024.